Mon. Not. R. Astron. Soc. **000**, 1–20 (2016) Printed 20 July 2016 (MN LATEX style file v2.2)

Feedback first: the surprisingly weak effects of magnetic fields, viscosity, conduction, and metal diffusion on galaxy formation

Kung-Yi Su[1]∗, Philip F. Hopkins[1], Christopher C. Hayward[1,2]†, Claude-André Faucher-Giguère[3], Dušan Kereš[4], Xiangcheng Ma[1], Victor H. Robles[5]

[1]*TAPIR 350-17, California Institute of Technology, 1200 E. California Boulevard, Pasadena, CA 91125, USA*
[2]*Harvard-Smithsonian Center for Astrophysics, 60 Garden Street, Cambridge, MA 02138, USA*
[3]*Department of Physics and Astronomy and CIERA, Northwestern University, 2145 Sheridan Road, Evanston, IL 60208, USA*
[4]*Department of Physics, Center for Astrophysics and Space Sciences, University of California at San Diego, 9500 Gilman Drive, La Jolla, CA 92093, USA*
[5]*Center for Cosmology, Department of Physics and Astronomy, University of California, Irvine, CA 92697, USA*

Submitted to MNRAS

ABSTRACT

Using high-resolution simulations with explicit treatment of stellar feedback physics based on the FIRE (Feedback in Realistic Environments) project, we study how galaxy formation and the interstellar medium (ISM) are affected by magnetic fields, anisotropic Spitzer-Braginskii conduction and viscosity, and sub-grid turbulent metal diffusion. We consider controlled simulations of isolated (non-cosmological) galaxies but also a limited set of cosmological "zoom-in" simulations. Although simulations have shown significant effects from these physics with weak or absent stellar feedback, the effects are much weaker than those of stellar feedback when the latter is modeled explicitly. The additional physics have no systematic effect on galactic star formation rates (SFRs). In contrast, removing stellar feedback leads to SFRs being over-predicted by factors of $\sim 10-100$. Without feedback, neither galactic winds nor volume filling hot-phase gas exist, and discs tend to runaway collapse to ultra-thin scale-heights with unphysically dense clumps congregating at the galactic center. With stellar feedback, a multi-phase, turbulent medium with galactic fountains and winds is established. At currently achievable resolutions, the additional physics investigated here (MHD, conduction, viscosity, metal diffusion) have only weak ($\sim 10\%$-level) effects on these properties and do not significantly alter the balance of phases, outflows, or the energy in ISM turbulence, consistent with simple equipartition arguments. We conclude that galactic star formation and the ISM are primarily governed by a combination of turbulence, gravitational instabilities, and feedback.

Key words: methods: numerical — MHD — conduction — turbulence — ISM: structure — ISM: jets and outflows

1 INTRODUCTION

Feedback from stars is essential to galaxy evolution. In isolated galaxy simulations without strong stellar feedback, giant molecular clouds (GMCs) experience runaway collapse, resulting in star formation rates (SFRs) orders-of-magnitude higher than observed (Bournaud et al. 2010; Dobbs et al. 2011; Harper-Clark & Murray 2011; Krumholz et al. 2011; Tasker 2011; Hopkins et al. 2011). This is in direct contradiction with the observed Kennicutt-Schmidt (KS) relation, which shows that the gas consumption time of a galaxy is roughly $\sim 50-100$ dynamical times (Kennicutt 1998; Zuckerman & Evans 1974; Williams & McKee 1997; Evans 1999; Evans et al. 2009). Cosmological simulations without strong feedback face a similar challenge. The efficiency of cooling causes runaway collapse of gas to high densities within a dynamical time, ultimately forming far too many stars compared to observations (Katz et al. 1996; Somerville & Primack 1999; Cole et al. 2000; Springel & Hernquist 2003; Kereš et al. 2009, and references therein).

Recent years have seen great progress in modeling feedback on galaxy scales (Thacker & Couchman 2000; Governato et al. 2007; Ceverino & Klypin 2009; Uhlig et al. 2012; Hopkins et al. 2011, 2012b,a; Agertz & Kravtsov 2015; Hu et al. 2015; Kim et al. 2014). In Hopkins et al. (2011, 2012b), a detailed feedback model including radiation pressure, stellar winds, supernovae and photoheating was developed and applied to simulations of isolated galaxies. They showed that stellar feedback is sufficient to maintain a self-regulated multi-phase interstellar medium (ISM), with global structure in good agreement with the observations. GMCs survive several dynamical times and only turn a few per cent of their mass into stars, and the galaxy-averaged SFR agrees well with the ob-

∗ E-mail: ksu@caltech.edu
† Moore Prize Postdoctoral Scholar in Theoretical Astrophysics

served Kennicutt-Schmidt (KS) law. These models were extended with numerical improvements and additional cooling physics, and then applied to cosmological "zoom in" simulations in the FIRE (Feedback In Realistic Environments) project[1]. A series of papers, using the identical code and simulation set have demonstrated that these feedback physics successfully reproduce a wide range of observations, including star formation histories of galaxies (Hopkins et al. 2014), time variability of star formation (Sparre et al. 2015), galactic winds (Muratov et al. 2015), HI content of galaxy halos (Faucher-Giguère et al. 2015; Faucher-Giguere et al. 2016; Hafen et al., in prep.), and galaxy metallicities (Ma et al. 2015). And other groups, implementing similar treatments of stellar feedback, have reached consistent conclusions (e.g., Stinson et al. 2013; Agertz & Kravtsov 2015).

However, several potentially important physical processes have not been included in most previous galaxy formation simulations. Magnetic fields have long been suspected to play a role in galaxy evolution because the magnetic pressure reaches equipartition with the thermal and turbulent pressures (Beck et al. 1996; Beck 2009). Isolated galaxy simulations with magnetic fields – but using more simplified models for stellar feedback – have been studied in various contexts and suggest that magnetic fields can provide extra support in dense clouds, thus slowing down star formation (Piontek & Ostriker 2005, 2007; Wang & Abel 2009; Beck et al. 2012; Pakmor & Springel 2013). Magnetic fields can also be important because of their effects on fluid mixing instabilities, including the Rayleigh-Taylor (RT) and Kelvin-Helmholtz (KH) instabilities (Jun et al. 1995; McCourt et al. 2015). These instabilities can potentially affect galaxy evolution through processes including the evolution of supernovae (SN) remnants (Jun & Norman 1996b,a; Jun & Jones 1999; Thompson 2000; Kim & Ostriker 2015).

Another potentially important effect is viscosity, which has been more extensively studied in simulations of galaxy clusters. It has been suggested that viscosity can affect the turbulent motion of the intracluster medium (ICM) or circum-galactic medium (CGM) and affect the KH stability of various structures in the ICM (Markevitch & Vikhlinin 2007). It has been shown in particular that viscosity may be important for the dynamics of bubbles in the ICM inflated by active galactic nucleus (AGN) feedback or bursts of SNe activity (Reynolds et al. 2005; Sijacki & Springel 2006).

Thermal conduction, which in the presence of magnetic fields is highly anisotropic, affects the stability of plasmas at both galactic and cluster scales (Sharma et al. 2009, 2010; Parrish et al. 2012; Choi & Stone 2012) and the survival and mixing of multi-phase fluids. Combined with the effect of magnetic fields, conduction may be critical to determine the survival of cool clouds in galactic winds.

Turbulent metal diffusion due to small-scale (un-resolvable) eddies may also have important effects. It has been suggested, for example, that unresolved turbulence in galaxy simulations may be important to effectively "diffuse" metals in the ISM and intergalactic medium (IGM; e.g., Shen et al. 2010), leading non-linearly to different cooling physics at halo centers and within the dense ISM.

While most previous studies considered these physics in isolation, their effects and relative importance may be quite different in a realistic multi-phase ISM shaped by strong stellar feedback processes. Another challenge is that conduction and viscosity in magnetized plasmas are inherently anisotropic. Properly treating this anisotropy requires MHD simulations and is numerically non-trivial; consequently, most previous studies on galactic scales have considered only isotropic conduction and viscosity. However, studies which correctly treat the anisotropy have shown that this anisotropy can produce orders-of-magnitude differences and, in some cases, qualitatively different behavior (Dong & Stone 2009; ZuHone et al. 2015; Sharma et al. 2009, 2010; Choi & Stone 2012)

In this paper, we study the effects of these different microphysics in the presence of explicit models for stellar feedback. While the simulations analyzed here implement the same stellar feedback physics from the FIRE cosmological simulations, we focus primarily on non-cosmological simulations of isolated galaxies, because this allows us to achieve higher spatial and mass resolution, and to have well-controlled experiments with identical galaxy initial conditions. In cosmological runs, on the other hand, the inherently chaotic nature of the problem makes detailed one-to-one comparison of simulations with varied physics more complicated; we do, however, include a limited subset of these experiments. We also make use of a new, more accurate hydrodynamic solver, needed to properly treat MHD and anisotropic diffusion.

Overall, we find that at the resolutions currently achievable in isolated galaxy and cosmological simulations, MHD, anisotropic conduction and viscosity, and sub-grid turbulent metal diffusion play a relatively minor role in the regulation of star formation and of the phases and energetics of the ISM *when the dominant effects of stellar feedback are simultaneously modeled*. We caution, however, that despite this result, some of these effects likely have some important and observationally interesting consequences on finer scales, such as for the survival of cool clouds in galactic winds (e.g., McCourt et al. 2015; Brüggen & Scannapieco 2016), and stellar abundance distribution patterns within star clusters or small galaxies. It is also possible that some important effects would only reveal themselves in simulations of much higher resolution than currently possible for galaxy simulations. Furthermore, the interaction of physical processes not included in our simulations with, e.g., magnetic fields is likely to prove important. This is the case in particular for the transport of cosmic rays, which a number of recent studies indicate may be an important form of feedback for galaxy evolution (e.g., Uhlig et al. 2012; Booth et al. 2013; Salem et al. 2014; Ruszkowski et al. 2016).

The remainder of this paper is organized as follows: in § 2, we describe the initial conditions and the baryonic physics model of our default model. In § 3, we summarize the additional physics studied in this paper. In § 4, we analyze the effects on the star formation histories, morphologies, phase structures, magnetic and turbulent energies, and outflows of our simulated galaxies. We discuss the reason why the fluid microphysics have minor effects in § 5 and conclude in § 6.

2 METHODOLOGY

Our simulations use GIZMO (Hopkins 2015b) [2], in its Meshless Finite Mass (MFM) mode. This is a mesh-free, Lagrangian finite-volume Godunov code designed to capture advantages of both grid-based and smoothed-particle hydrodynamics (SPH) methods built on the gravity solver and domain decomposition algorithms of GADGET-3 (Springel 2005). The numerical details of the hydrodynamic and MHD versions of the method are presented in Hopkins (2015b), Hopkins & Raives (2016), and Hopkins (2015a). Hopkins (2016) present tests of the anisotropic diffusion operators

[1] Project web site: http://fire.northwestern.edu.

[2] A public version of this code is available at *http://www.tapir.caltech.edu/~phopkins/Site/GIZMO.html*.

used in our code. Extensive comparisons of dozens of test problems demonstrate good code behavior and convergence, in good agreement with state-of-the-art moving mesh codes (e.g. AREPO, Springel 2010) and grid codes (e.g. ATHENA, Stone et al. 2008), including on historically difficult problems such as those featuring the magneto-rotational instability (MRI), magnetic jet launching, and the KH and RT fluid-mixing instabilities. Convergence tests for our isolated galaxy simulations can be found in Appendix A.

Note that, for the sake of consistency, all previously published FIRE simulations (see references in § 1) were run with the identical source code, using GIZMO's "P-SPH" hydrodynamic solver. P-SPH is an SPH method with improvements designed to address some of the known shortcomings of SPH in treating e.g. fluid mixing instabilities (see Hopkins 2013). This was done to facilitate comparison by matching exactly the code used for the first FIRE paper, Hopkins et al. (2014), written before the MFM methods were developed. Unfortunately, as shown in Hopkins & Raives (2016) and Hopkins (2016), P-SPH (while reasonably well-behaved on pure hydrodynamics problems) exhibits serious inaccuracies and may not converge on MHD and anisotropic diffusion problems. As a consequence, P-SPH *cannot* be used for our study here. We are therefore careful to distinguish our isolated galaxy simulations here from the primary "FIRE project" simulations, although they use the same (operator-split) code modules to treat stellar feedback. In fact, the updated code here - the "FIRE - 2" code, will be the subject of an extensive methods paper in preparation (Hopkins et al., in preparation). A detailed study of the effects of the hydrodynamic method and other numerical details on the conclusions from the previous FIRE simulations will be the subject of that paper.

2.1 Initial conditions (ICs)

In this paper, five isolated (non-cosmological) galaxy models are studied to consider a range of characteristic galaxy types. Two cosmological zoom-in ICs are also included as a check that our conclusions are applicable in a fully cosmological environment. More details regarding the isolated disc galaxies and the cosmological simulations can be found in Hopkins et al. (2011, 2012b) and Hopkins et al. (2014), respectively, and are summarized in Table 1 and below. For all runs, a flat ΛCDM cosmology with $h = 0.702$, $\Omega_M = 1 - \Omega_\Lambda = 0.27$, and $\Omega_b = 0.046$ is adopted.

Note that we have tested simulations with most of our ICs re-run at different resolution, with initial gas particle mass differing by a factor ~ 100. Some absolute properties do vary according to the resolution. For example, finer ISM substructure is observed and some higher density regions are resolved as the resolution increases. Nonetheless, the main conclusions of this paper (the *relative* differences in runs with different microphysics) remain robust at all resolutions investigated. A detailed convergence study is presented in Appendix A.

The ICs studied here include:

2.1.1 *HiZ*

HiZ is a high-redshift massive starburst disc galaxy designed to match the properties of non-merging, rapidly star-forming sub-millimeter galaxies (Erb et al. 2006; Genzel et al. 2008; Tacconi et al. 2010), with halo mass $M_{\rm halo} = 2.1\times10^{12}$ M$_\odot$ in a Hernquist (1990) profile with an NFW (Navarro et al. 1996)-equivalent concentration of $c = 3.5$. The baryonic component has a total mass of $M_{\rm bar} = 1.53\times10^{11}$ M$_\odot$ and consists of an exponential bulge ($\rho(r) \propto \exp(-r/a)/r$) ($M_b = 10^{10}$ M$_\odot$) with scale length $a = 1.7$ kpc and exponential stellar ($M_d = 4.3\times10^{10}$ M$_\odot$) and gas ($M_g = 1\times10^{11}$ M$_\odot$) discs with scale lengths $r_d = 2.3$ kpc and $r_g = 4.6$ kpc respectively. The gas disc initially has Toomre $Q = 1$ uniformly. Note that the virial radius is scaled for a halo at redshift $z = 2$ instead of $z = 0$. This model uses 1.65×10^7 particles, 4×10^6 of which are gas particles.

2.1.2 *Sbc*

Sbc is a $z = 0$ dwarf starburst intended to be representative of local luminous infrared galaxies (LIRGs). The IC is composed of a dark matter halo with $(M_{\rm halo}, c) = (2.1\times10^{11}{\rm M}_\odot, 11)$ and a baryonic component with masses $(M_{\rm bar}, M_b, M_d, M_g) = (15, 1.4, 5.7, 7.9)\times10^9{\rm M}_\odot$ and scale lengths $(r_d, r_g, a) = (1.9, 3.7, 0.5)$ kpc. The bulge has an exponential profile. This model includes 1.7×10^7 particles, 3×10^6 of which are gas particles.

2.1.3 *MW*

MW is a Milky Way-like galaxy composed of a dark matter halo with $(M_{\rm halo}, c) = (2.1\times10^{12}$ M$_\odot$, 12) and baryonic components with $(M_{\rm bar}, M_b, M_d, M_g) = (1.02, 2.1, 6.8, 1.3)\times10^{10}{\rm M}_\odot$ respectively. The scale lengths are $(r_d, r_g, a) = (4.3, 8.6, 1.4)$kpc. The bulge follows a Hernquist (1990) profile. The model includes 1.03×10^7 particles, 3.6×10^6 of which are gas particles.

2.1.4 *SMC*

SMC is an isolated (field) Small Magellanic Cloud-mass dwarf galaxy composed of a halo with $(M_{\rm halo}, c) = (2.9\times10^{10}$ M$_\odot$, 15) and baryonic components with masses $(M_{\rm bar}, M_b, M_d, M_g) = (13, 0.14, 1.9, 11)\times10^8$ M$_\odot$ and scale lengths $(r_d, r_g, a) = (1, 3.9, 1.9)$ kpc. The bulge follows a Hernquist (1990) profile. There are 1.33×10^7 particles, 3×10^6 of which are gas particles.

2.1.5 *Ell*

Ell is an elliptical galaxy with halo and disc/bulge baryonic properties $(M_{\rm halo}, c) = (1.4\times10^{13}{\rm M}_\odot, 6)$ and $(M_{\rm bar}, M_b, M_d, M_g) = (15, 14, 1.4, 0.1)\times10^{10}{\rm M}_\odot$, respectively. The baryonic components have scale lengths $(r_d, r_g, a) = (4.0, 4.3, 3.9)$ kpc. The bulge obeys a Hernquist (1990) profile. Besides the gas disc, this galaxy contains an extended hot gas halo of mass $M_{\rm gas} = 8.6\times10^{11}\,M_\odot$, initialized with a spherically-symmetric β profile with core radius equal to the halo scale radius and $\beta = 3/2$, with an initial temperature profile given by hydrostatic equilibrium and a small angular momentum corresponding to a spin parameter $\lambda = 0.033$. We use 3×10^7 particles, 1.2×10^7 of which are gas particles.

2.1.6 *CosmoMW*

CosmoMW is a fully cosmological zoom-in simulation from the suite presented in Hopkins et al. (2014), specifically the **m12i** simulation therein, chosen because it produces a galaxy with stellar mass and morphology similar to the Milky Way. The run uses the zoom-in method (Porter 1985; Katz & White 1993) to follow the formation history of the galaxy from an initial redshift $z > 100$ to $z = 0$. The main halo has a total mass of $\sim 10^{12}{\rm M}_\odot$ at $z = 0$ and a typical merger and growth history for halos of its mass. We use 2.07×10^7 total particles (8.82×10^6 gas). For this analysis, we only follow the most-massive main-progenitor halo (i.e. the center of the zoom-in region) and focus on the particles in the central region (defined as < 0.1 virial radius).

Table 1. Galaxy models

Model	ϵ_g (pc)	m_g ($M_\odot$)	$M_{\rm halo}$ ($M_\odot$)	c	$V_{\rm Max}$ (km/s)	$M_{\rm bar}$ ($M_\odot$)	M_b ($M_\odot$)	Bulge profile	a (kpc)	M_d ($M_\odot$)	r_d (kpc)	M_g ($M_\odot$)	r_g (kpc)
HiZ	1.4	2.5e4	2.1e12	3.5	280	1.53e11	1.0e10	Exp	1.7	4.3e10	2.3	1.0e11	4.6
Sbc	1.4	2.6e3	2.1e11	11	120	1.5e10	1.4e9	Exp	0.5	5.7e9	1.9	7.9e9	3.7
MW	3.6	3.5e3	2.1e12	12	250	1.02e10	2.1e10	Hq	1.4	6.8e10	4.3	1.3e10	8.6
SMC	0.7	3.6e2	2.9e10	15	67	1.3e9	1.4e7	Hq	2.1	1.9e8	1.0	1.1e9	3.0
Ell	4.2	7.1e4	1.4e13	6	240	1.02e12	1.4e11	Hq	3.9	1.4e10	4.0	8.6e11	4.0
CosmoMW	7	5.7e4	1.2e12	8	290	1.3e11	-	-	-	1.2e11	1.2	7.1e9	2.5
CosmoDwarf	3	2.6e2	7.9e9	9.7	20	5.2e6	-	-	-	1.7e6	-	3.5e6	-

Parameters of the galaxy models studied here (§ 2.1):
(1) Model name. HiZ: high-redshift, massive starburst. Sbc: local gas-rich dwarf starburst. MW: Milky-Way analogue. SMC: SMC-mass dwarf. Ell: massive elliptical with an extended gaseous halo. HiZ, Sbc, MW, SMC, and Ell are non-cosmological (isolated galaxy) simulations. CosmoMW: cosmological simulation of a MW-mass disc galaxy. CosmoDwarf:cosmological simulation of a dwarf galaxy. (2) ϵ_g: Gravitational force softening for gas (the softening for gas in all simulations is adaptive; this is the minimum value). (3) m_g: Gas particle mass. (4) $M_{\rm halo}$: Halo mass. M_{vir} for CosmoMW and CosmoDwarf. (5) c: NFW-equivalent halo concentration. (6) $V_{\rm max}$: Halo maximum circular velocity. (7) $M_{\rm bar}$: Total baryonic mass. It is the sum of gas, disk, bulge and stellar mass for isolated galaxy runs, and the sum of gas and stellar mass in the cosmological runs within 0.1 virial radius. (8) M_b: Bulge mass. (9) Bulge profile: Hq: Hernquist (1990), or Exp: Exponential. (10) a: Bulge scale-length. (11) M_d : Stellar disc mass. For CosmoMW and CosmoDwarf runs, this is the total stellar mass within 0.1 virial radius. (12) r_d : Stellar disc scale length. (13) M_g: Gas disc mass. For the Ell runs, this includes gas in the extended halo. For CosmoMW and CosmoDwarf runs, this is the total gas mass within 0.1 virial radius. (14) r_g: Gas disc scale length.
The properties quoted for CosmoMW and CosmoDwarf are the $z = 0$ values measured from the "default" run. The CosmoDwarf does not have a well-defined disk even at $z = 0$, but is a dwarf irregular galaxy.

2.1.7 *CosmoDwarf*

CosmoDwarf is a another cosmological zoom-in from Hopkins et al. (2014), specifically the **m10q** simulation, chosen to be a representative dwarf galaxy – specifically one with a $z = 0$ halo mass of $\sim 10^{10}\,{\rm M}_\odot$ and typical merger and growth history. We use 3.87×10^7 total particles (1.57×10^7 gas). Again we focus only on the main progenitor galaxy.

2.2 Cooling, star formation, and stellar feedback

The baryonic physics of cooling, star formation, and stellar feedback follow the implementation in Hopkins et al. (2014). In what follows, we summarize the key aspects and focus on the new physics added for this study.

2.2.1 *Cooling*

Cooling is followed from 10^{10} K to 10K, with 11 separately tracked species followed species-by-species (see e.g. Wiersma et al. 2009a). The low-temperature (metal fine-structure and molecular) cooling rates and ionization state are tabulated from a compilation of CLOUDY runs (as in Wiersma et al. 2009a; Robertson & Kravtsov 2008), including the effects of a redshift-dependent photo-ionizing background (from Faucher-Giguère et al. 2009) and local ionizing sources as described below.

2.2.2 *Star formation*

Star formation is allowed only from gas that is locally self-gravitating (where we follow Hopkins et al. 2013c to estimate the local virial criterion at each point in the simulation), is self-shielding molecular (where the molecular fraction is estimated following Krumholz & Gnedin 2011), and exceeds a density $n > 100\,{\rm cm}^{-3}$. If these criteria are met, stars form with a rate $\dot{\rho}_\star = \rho_{\rm mol}/t_{\rm freefall}$. In previous studies of these star formation models, we have shown that, provided stellar feedback is explicitly included and the largest fragmentation scales in the galaxy are resolved, the galactic star formation rates and histories are regulated by stellar feedback and are insensitive to changes in these criteria (as well as more complicated chemical or temperature-based star formation models); see Hopkins et al. (2011, 2012b, 2013c); Faucher-Giguère et al. (2013). We have confirmed these studies explicitly with our ICs and simulations both including and excluding the additional microphysics we study here.

2.2.3 *Stellar feedback*

A star particle inherits its metallicity from its parent gas particle, and is treated as a single stellar population. The feedback quantities (including luminosity, SN rates, mass and metal loss rates, etc.) are tabulated from STARBURST99 (Leitherer et al. 1999) assuming a Kroupa (2002) IMF. Our stellar feedback model includes the following processes: (1) an approximate treatment of local and long-range momentum deposition from radiation pressure, including both initial single-scattering of optical/UV photons and (potentially) multiple-scattering of IR photons; (2) SNe (Types Ia and II), which occur stochastically according to the tabulated rates and, when they occur, deposit the appropriate ejecta energy, momentum, mass, and metals into the surrounding gas particles; (3) stellar winds from O-stars and AGB stars, which are treated similarly to SNe except that the injection is continuous; (4) photo-ionization and photo-electric heating, with each star particle acting as a source, using the approximate radiative transfer algorithm noted above.

3 ADDITIONAL PHYSICS

3.1 Magnetic fields (MHD)

We treat magnetic fields in the ideal-MHD limit, using the GIZMO implementation described in Hopkins & Raives (2016). The tests described in Hopkins & Raives (2016) show that this MHD implementation correctly captures traditionally difficult phenomena such as the growth rates of the magneto-rotational instability (MRI), magnetic jet launching by discs, and magnetized fluid mixing (RT and KH) instabilities. Compared to SPH MHD methods, this method is generally significantly more accurate and exhibits good convergence properties. Compared to state-of-the-art grid codes (e.g., ATHENA; Stone et al. 2008), the methods here typically exhibit faster convergence in the problems where advection, angular

momentum conservation, self-gravity and/or following large compression are important (problems where Lagrangian methods have advantages).

When magnetic fields are present, the homogenous Euler equations of hydrodynamics are replaced by their MHD versions. In a reference frame with velocity $\mathbf{v}_{frame}$, they can be written as a set of hyperbolic PDEs of the form

$$\frac{\partial \mathbf{U}}{\partial t} + \nabla \cdot (\mathbf{F} - \mathbf{v}_{frame} \otimes \mathbf{U}) = \mathbf{S}, \quad (1)$$

where $\mathbf{U}$ is the state vector of the conserved quantities, $\mathbf{F}$ is the flux vector of the conserved variables, and $\mathbf{S}$ is the source vector. In the pure MHD case, $\mathbf{U}$ and $\mathbf{F}$ can be written in the form

$$\mathbf{U} = \begin{pmatrix} \rho \\ \rho\mathbf{v} \\ \rho e \\ \mathbf{B} \end{pmatrix}$$

$$\mathbf{F} = \begin{pmatrix} \mathbf{F}_\rho \\ \mathbf{F}_P \\ \mathbf{F}_e \\ \mathbf{F}_B \end{pmatrix} := \begin{pmatrix} \rho\mathbf{v} \\ \rho\mathbf{v}\otimes\mathbf{v} + P_T\mathcal{I} - \mathbf{B}\otimes\mathbf{B} \\ (\rho e + P_T)\mathbf{v} - (\mathbf{v}\cdot\mathbf{B})\mathbf{B} \\ \mathbf{v}\otimes\mathbf{B} - \mathbf{B}\otimes\mathbf{v} \end{pmatrix}, \quad (2)$$

where ρ is the density, $e = u_{int} + |\mathbf{B}|^2/2\rho + |\mathbf{v}|^2/2$ is the total specific energy, and $P_T = P + |\mathbf{B}|^2/2$ is the total pressure.

To clean the non-zero $\nabla \cdot B$ resulting from numerical errors, a combination of the Dedner et al. (2002) and Powell et al. (1999) cleaning methods are applied in GIZMO, with important modifications for the Lagrangian nature of the code (see Hopkins & Raives (2016) for detail). In all our ICs we seed the simulation volume with a uniform initial magnetic field in the direction of the galaxy angular momentum vector. For our cosmological runs (CosmoMW and CosmoDwarf), this is a trace (sub-nG) initial field that is quickly amplified even before galaxies form. For isolated discs, we initially set $\sim 10^{-2}\,\mu$G fields, but these are quickly amplified and dominated by the field built up through a combination of the MRI, the supersonic turbulent dynamo, and the galactic fountain dynamo. For our "Ell" run, we also initialize the gas in the extended galactic halo with a purely azimuthal field in equipartition with the thermal energy (set to be in hydrostatic equilibrium).

3.2 Anisotropic conduction

Thermal conduction is incorporated into the Euler equations as an extra diffusion term in $\mathbf{F}_e$ from equation (2), following the standard Spitzer-Braginskii form. This means the conduction term added to $\mathbf{F}_e$ is $\kappa\,(\hat{\mathbf{B}}\otimes\hat{\mathbf{B}})\cdot\nabla T$, where $\hat{\mathbf{B}}$ is the unit vector along the corresponding magnetic field. $\hat{\mathbf{B}}\otimes\hat{\mathbf{B}}$ in the expression serves as a projection operator constraining the conduction energy flux to follow the magnetic field lines and makes the thermal conduction anisotropic.

The anisotropic conduction equation is solved and consistently implemented into the MFM/MFV methods in GIZMO. Hopkins (2016) presents tests confirming that the method is numerically stable, converges with second-order accuracy (as the MHD method in GIZMO itself does), and is capable of fully anisotropic configurations (i.e. the conductive flux vanishes identically when $\hat{\mathbf{B}}$ and ∇T are perpendicular).

Instead of setting the conduction coefficient κ by hand, we calculate it self-consistently as the Spitzer conductivity (Spitzer & Härm 1953; Sarazin 1988; Zakamska & Narayan 2003; ZuHone et al. 2015; Kannan et al. 2016) with the form

$$\kappa = \frac{0.96 k_B (k_B T)^{5/2}}{m_e^{1/2} e^4 \ln\Lambda} \frac{F_i}{1 + 4.2\ell_e/\ell_T} = \frac{4.87\times10^{-7} F_i}{1 + 4.2\ell_e/\ell_T} T^{5/2} \quad [\mathrm{erg\ s^{-1} K^{-1} cm^{-1}}], \quad (3)$$

where F_i is the ionized fraction (computed self-consistently in our cooling routines), $\ln\Lambda \sim 37$ is the Coulomb logarithm, $\ell_e \equiv 3^{3/2}(k_B T)^2/4 n_e \sqrt{\pi} e^4 \ln\Lambda$ is the electron mean free path, and $\ell_T \equiv T/|\nabla T|$ is the temperature gradient scale length. The denominator accounts for saturation of κ, which occurs when electrons have large mean-free-paths (it limits the gradient scale length to the mean-free-path (Cowie & McKee 1977; Sarazin 1988; Kannan et al. 2016)). The steep temperature dependence indicates that conduction is more efficient in hotter gas.

3.3 Anisotropic viscosity

Viscosity is incorporated into MHD through the Navier-Stokes equations, which modify the momentum flux and the energy flux in the Euler equations as

$$\mathbf{F}_P = \rho\mathbf{v}\otimes\mathbf{v} + P_T\mathcal{I} - \mathbf{B}\otimes\mathbf{B} + \Pi$$
$$\mathbf{F}_e = (\rho e + P_T)\mathbf{v} - (\mathbf{v}\cdot\mathbf{B})\mathbf{B} + \Pi\cdot\mathbf{v}. \quad (4)$$

For MHD, the anisotropic viscosity again follows the Spitzer-Braginskii anisotropic form, in which the viscious flux Π is

$$\Pi = -3\eta\left(\hat{\mathbf{B}}\otimes\hat{\mathbf{B}} - \frac{1}{3}\mathcal{I}\right)\left(\hat{\mathbf{B}}\otimes\hat{\mathbf{B}} - \frac{1}{3}\mathcal{I}\right) : \nabla\mathbf{v}, \quad (5)$$

where ":" is defined by $\mathbf{A} : \mathbf{B} \equiv \mathrm{Tr}(\mathbf{A}\cdot\mathbf{B})$. Anisotropic viscosity is also solved and consistently implemented in the MFM/MFV methods of GIZMO, with the same convergence and stability properties as anisotropic conduction.

The viscous coefficients are calculated self-consistently as the leading-order Braginskii viscosity (Braginskii 1965; Sarazin 1988; Sijacki & Springel 2006; ZuHone et al. 2015), where the shear viscosity coefficient is

$$\eta = 0.406 \frac{m_i^{1/2}(k_B T)^{5/2}}{(Ze)^4 \ln\Lambda} \frac{F_i}{1 + 4.2\ell_e/\ell_T} = \frac{4.5\times10^{-17} F_i}{1 + 4.2\ell_e/\ell_T} T^{5/2} \quad [\mathrm{g\ s^{-1} cm^{-1}}], \quad (6)$$

and the bulk viscosity vanishes. Here, m_i is the average ion mass and m_e is the electron mass.

3.4 Smagorinski (sub-grid eddy) models for metal diffusion

Metal mixing on large scales is resolved in the simulation. However, since our code is strictly Lagrangian, mass elements (including metals) are conserved on a per-particle basis unless they are injected directly by SNe or stellar winds. This limits spurious numerical diffusion but implies that un-resolved small-scale diffusion between particles is ignored.

Sub-grid models have been proposed to model this unresolved transport. Because the systems we are simulating generally have extremely high Reynolds numbers, the un-resolved diffusion is usually dominated by small turbulent eddies rather than e.g. Brownian motion. The former is commonly approximated (see e.g. Shen et al. 2010) following Smagorinsky (1963) by treating

the metals as a passive scalar which obey the following diffusion equation:

$$\frac{\partial \mathbf{M}_i}{\partial t} + \nabla \cdot (D \nabla \mathbf{M}_i) = 0$$
$$D = C ||\mathbf{S}||_f \mathbf{h}^2, \quad (7)$$

where $\mathbf{h}$ is the resolution scale (at which the sub-grid model acts; here, it is the mean inter-particle separation within the kernel function, the equivalent of the cell size Δx in Eulerian codes) and C is the Smagorinsky-Lilly constant, calibrated from direct numerical simulations. C usually ranges from 0.1 to 0.2 (Smagorinsky 1963; Lilly 1967; Wadsley et al. 2008) and is set to be 0.15 in our simulation. $\mathbf{S}$ is the symmetric traceless shear tensor defined as

$$\mathbf{S} = \frac{1}{2}(\nabla \mathbf{v} + (\nabla \mathbf{v})^T) - \frac{1}{3}\mathrm{Tr}(\nabla \mathbf{v}), \quad (8)$$

for which the diffusion vanishes in purely compressive or rotating flows. The norm in the expression is the Frobenius norm.

This model for sub-grid metal diffusion is implemented in GIZMO following Shen et al. (2010). However, because our resolution is much higher than many of the simulations in which it has been used before, the sub-grid diffusivity is much smaller. Moreover, we stress the importance of proper calibration of the constant C, which can change the diffusivity by factors of ~ 100. We also caution that, as we will show in detail in a forthcoming work, this estimator can be very noisy in SPH methods (unlike the finite-volume methods used here), owing to zeroth-order errors in the SPH gradient estimator triggering artificial diffusion. Finally, we stress that this model assumes the motion seen in $\mathbf{S}$ is entirely due to turbulent flows. If there is real bulk motion (e.g. shear in a self-gravitating disc), this estimator will be triggered artificially. Therefore the estimated turbulent diffusivity using this simplistic sub-grid model is almost certainly an over-estimate of the real turbulent diffusivity. In future work, we will present a detailed study attempting to calibrate and rescale this model for situations where the contribution from galactic rotation is important on the resolution scale (Colbrook et al., in prep.). Our preliminary work suggests this estimator may over-estimate the true diffusivity by an order of magnitude in some cases.

4 RESULTS

We simulate the ICs detailed in § 2.1 with four distinct combinations of physics:

- **Default**: Stellar feedback is included, but the additional microphysics (MHD, conduction, viscosity, metal diffusion) are not.
- **No Feedback**: Stellar feedback is not included (cooling, star formation, and self-gravity are, however). No additional microphysics (MHD, conduction, viscosity, metal diffusion) are included.
- **MHD**: Stellar feedback and MHD are included, but additional diffusion microphysics (conduction, viscosity, metal diffusion) are not.
- **All Microphysics**: Stellar feedback, MHD, and the additional diffusion operators (conduction, viscosity, metal diffusion) are all included.

We analyze these four variants for each of the ICs below, with two exceptions: the two cosmological runs with no feedback are prohibitively expensive. We are able to run the simulation to $z \sim 6$, where the extremely high-density objects formed via the high star formation efficiencies in the absence of feedback force exceedingly small timesteps. However, some weak-feedback variations of the CosmoMW IC and the CosmoDwarf IC are presented in Hopkins et al. (2014); these are consistent with all of our other conclusions in this paper regarding the role of feedback.

Cosmological simulations are highly nonlinear and evolved for the entire age of the Universe. Because the equations (even of gravity alone) are formally chaotic, a small perturbation can be amplified and result in surprisingly large differences at low redshift, making it nontrivial to distinguish the physical effects of fluid microphysics from stochastic effects. In each of the following CosmoMW plots, we estimate the magnitude of stochastic effects from 5 independent CosmoMW default runs with small variations in the SNe coupling scheme (effectively we randomly "re-shuffle" the fraction of the SNe energy and momentum each neighbor particle sees, to generate random perturbations to the system). These differences have minor systematic effects on the stellar mass formed but serve the intended purpose of introducing small perturbations between the calculations. The shaded regions in the plots indicate the regions of parameter space spanned by these 5 runs. Although, we do not have the same statistical sample for CosmoDwarf, the stochastic effects there are likely to be of similar size to those in the CosmoMW simulations.

4.1 Star formation histories

Fig. 1 shows the star formation histories of the five isolated galaxies, CosmoMW, and CosmoDwarf, evolved under the different combinations of physics described above. The SFRs of HiZ, Sbc, MW, SMC and Ell shown in Fig. 1 are the values averaged over 20 million years, and the SFRs of CosmoMW and CosmoDwarf are averaged over roughly 100 million years (to make systematic, as opposed to stochastic, differences clear). To further suppress the stochastic effects, the stellar mass as a function of time is also plotted in Fig. 2.

Without stellar feedback, the SFRs are generally higher than observed by factors of $\sim 10 - 100$. On the other hand, the additional physics we consider changes the SFR by $\lesssim 10\%$. We have also confirmed that the predicted Kennicutt-Schmidt (KS) relation is insensitive to the additional microphysics in the simulations (and in agreement with observations, as in our previous simulations with the FIRE feedback physics).

The largest effect caused by fluid microphysics can be observed in the CosmoDwarf all-microphysics run, in which the stellar mass is systemically higher than that in the default run by a factor of ~ 1.5. We argue below that this is most likely to be a consequence of conduction, which can increase the efficiency of cooling when multiple SNe remnants overlap (and overrun small cold gas clumps in the galaxy), thereby dissipating the hot gas energy going into galactic winds slightly more efficiently.

Compared with the other galaxies, the differences in SFRs are smallest among the different Ell simulations (the SFR in the no-feedback run is never more than an order-of-magnitude greater than the SFRs in the variants that include explicit stellar feedback). The reason is that in Ell, the gas disc contributes $< 1\%$ of the total gas mass, while the majority is distributed in a hot gas halo. The cooling efficiency of the hot halo gas onto the star-forming disc therefore controls the gas supply available for star formation and becomes an important regulator of the SFR besides stellar feedback.

Although magnetic fields have been suggested in the literature as a mechanism to suppress star formation owing to their additional pressure (Piontek & Ostriker 2005, 2007; Wang & Abel 2009; Pakmor & Springel 2013; Beck et al. 2012), we actually see a small hint of systemically higher stellar mass in the MHD runs. The difference is more obvious in the smaller galaxies like CosmoDwarf

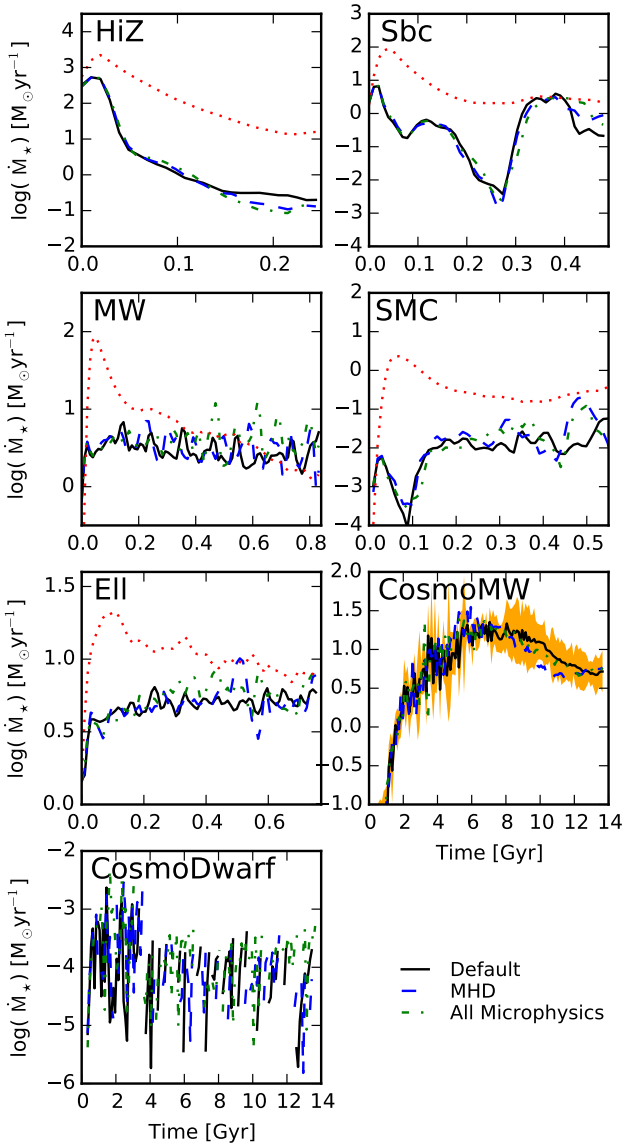

Figure 1. Star formation rates (SFRs) as a function of time in each of our simulations (each IC from Table 1, as labeled) smoothed over 20 Myr for isolated galaxy simulations and 100 Myr for cosmological simulations so that systematic differences are clearer. HiZ (massive starburst), Sbc (dwarf starburst), MW (Milky-Way analogue), SMC (SMC-mass dwarf), and Ell (massive elliptical with a "cooling flow" halo) are all isolated (non-cosmological) simulations and are thus run for only a few galaxy dynamical times. Because the CosmoMW and CosmoDwarf runs are fully cosmological zoom-in runs of a MW-mass halo and a dwarf halo, the full evolution is shown. In each, we consider four cases: default (stellar feedback, no additional microphysics), default+MHD ("MHD"), default+MHD+anisotropic conduction and viscosity+sub-grid turbulent metal diffusion ("all microphysics"), and a run without stellar feedback ("no feedback"). In the CosmoMW case, the orange shaded region indicates the range of stochastic effects (see §4). The no-feedback runs predict much higher SFRs at early times (in conflict with observations) until they gas-exhaust at late times. Once feedback is included, a lower, steady-state SFR emerges; the SFR has relatively small dependence on the different microphysics considered (up to stochastic effects). However, a more steady star formation history can be observed in the CosmoDwarf all-microphysics run, resulting in a slightly higher SFR on average.

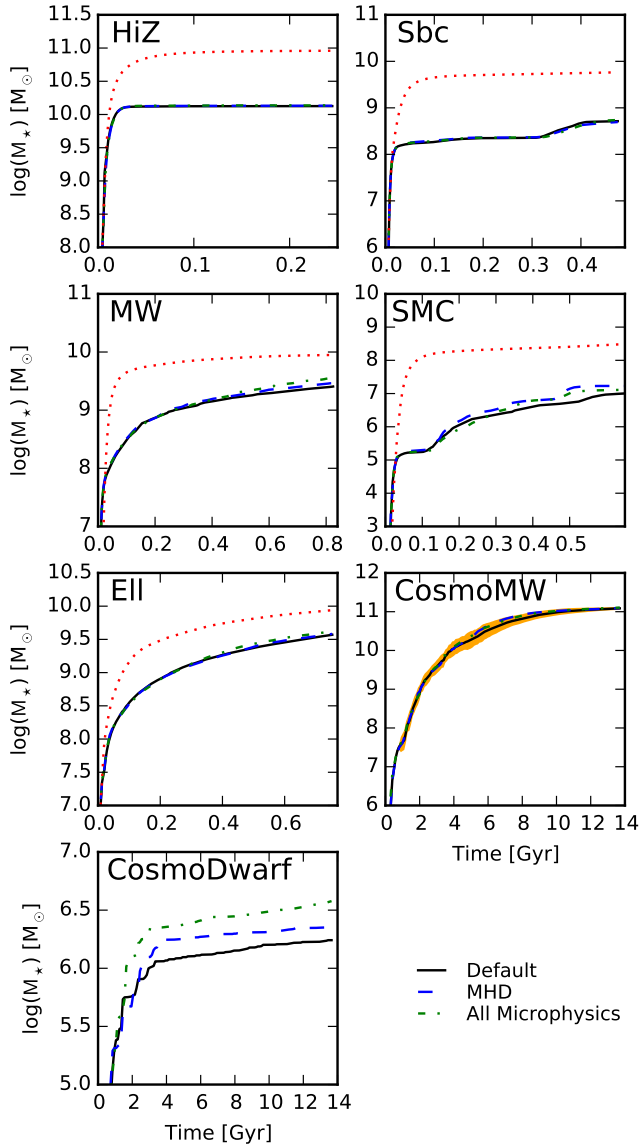

Figure 2. Total stellar mass as a function of time in each of our simulations (each IC from Table 1, as labeled). The orange shaded region in CosmoMW again indicates the range of stochastic effects. Fluid microphysics has little effect on the stellar mass formed in our simulations, in contrast to stellar feedback, which reduces the stellar mass formed by about an order of magnitude relative to the no-feedback runs. However, a small hint of higher stellar mass can be observed in the runs with magnetic fields, and in the CosmoDwarf simulations, the all-microphysics run has stellar mass a factor of ~ 1.4 higher than the MHD run. These effects are generally smaller than systematic uncertainties in feedback (e.g. SNe rates).

and SMC. But even in these cases, the difference is less than 0.1 dex despite the fact that magnetic field strengths consistent with observations are self-consistently obtained. We discuss this point further below. We note, however, that magnetic fields may still play a more important role in regulating the formation of individual stars (which is unresolved in our simulations).

4.2 Morphologies

Fig. 3 and Fig. 4 shows the face-on and edge-on gas morphologies of our simulated galaxies after some dynamical evolution. The CosmoMW runs and CosmoDwarf runs are shown at $z \sim 0$. Owing to the lack of disk structure, only one viewing angle of CosmoDwarf is plotted. The no-feedback runs again show fundamental differences from the other runs (which incorporate explicit stellar feedback) owing to the runaway collapse of gas. Generally speaking, turning off feedback significantly suppresses the volume-filling hot gas and increases the cold gas fraction, implying a much higher cooling efficiency and SFR. In the face-on images of the no-feedback runs, the numbers of cold clumps and filaments clearly outnumber those in the other runs by orders of magnitude, especially around the galactic centers in the star-forming discs. In the edge-on images, the discs are clearly thinner. There is still turbulence driven by fragmentation, but it is unable to extend to thicker galactic fountains.

On the other hand, once stellar feedback is included, there is no significant systematic difference among runs with different additional physics. Stochastic SNe events can make some parts of some of the variants hotter at the times shown in the figure, but there is little systematic difference in a time-averaged sense. Although the CosmoMW all-microphysics run seems to have a slightly more extended disk in the edge-on image at $z \sim 0$, it is likely to be a result of the stochastic variations in the exact timing of the last gas-rich merger/accretion event, instead of the effect of fluid microphysics. Among the different galaxies, Ell stands out as an exception for having little variation even between the runs with and without feedback. This is because cooling from the hot halo gas plays an important role in regulating Ell, as discussed above.

4.3 Gas phase structure

Fig. 5, Fig. 6 and Fig. 7 compare the temperature-density phase plots of our isolated and cosmological simulations, respectively. The gas mass in each phase is further quantified in Fig. 8, Fig. 9 and Fig. 10, where the density distributions in the following temperature intervals are plotted: cold neutral ($0 - 8000$ K), warm ionized ($8000 - 10^5$ K) and hot ($> 10^5$ K).

With stellar feedback, a multi-phase ISM is established, with star-forming cold atomic/molecular gas, warm ionized gas, and volume-filling hot gas. The phase structure of simulations using a similar implementation of our "default" physics is analyzed in extensive detail in Hopkins et al. (2011, 2012b,a, 2013d); our results here are consistent with those. Most of the mass is in a combination of a cold neutral medium, which appears at high densities when gas becomes self-shielding, and a warm ionized medium maintained at $\sim 10^4$ K by photo-heating. The warm phase dominates in all cases except Ell, in which the gas from the hot halo dominates. The upper part of the phase diagram is populated by volume-filling hot gas that is heated up and pushed out of the disc by stellar feedback (the only exception is Ell, for which the hot gas halo included in the IC dominates this region of the plot). Turing off stellar feedback, on the other hand, leads to the same results as discussed in § 4.2.

Runs with the standard stellar feedback but different additional physics are very similar. Although magnetic fields, viscosity and conduction can in principle alter the cooling efficiency and fluid mixing, these additional physics have less than a $\sim 10\%$ effect on the balance of ISM phases in our simulations.

There is a small difference in our CosmoDwarf runs, where the cold gas mass is larger in our all-microphysics run by ~ 0.2 dex ($\sim 50\%$) This is consistent with the slightly higher SFR in that run.

4.4 Magnetic and turbulent energies

Fig. 11 compares the turbulent and magnetic energies in these simulations. The "turbulent" energy is difficult to define in practice, since we wish to exclude non-circular bulk motions and galactic winds. For our isolated galaxies, we focus on the galactic disc by taking a cylinder with radius 10 kpc and height 2 kpc centered on the disc. The cylinder is divided into annuli with thicknesses set so that the number of particles in each layer is proportional to the order of layer counted from inside out. Within each annulus, the average rotational velocity is subtracted, and the particles outside with the highest 32% $|v_z - \bar{v}_z|^2$ are excluded (to approximate an $\pm 1\sigma$ interval) to eliminate outflows in the z direction. Each annulus is then further divided into cells with volumes set so each of them contain roughly 15 gas particles. The dimensions of the cells are chosen so that if all gas particles were distributed uniformly within the cylinder, each cell would be a cube ($\ell_r = \ell_z = \ell_\theta$) with an identical volume. Within each cell, the average velocity in $\hat{r}$, $\hat{z}$ and $\hat{\phi}$ directions are subtracted, and particles with the highest 32% $|\mathbf{v} - \bar{\mathbf{v}}|^2$ are excluded to reduce the contamination from the remaining high-velocity tail resulting from outflows in all directions. The kinetic energy that remains defines our estimated "turbulent" energy. [3]

For CosmoMW, which has no well-defined disc structure until $z \lesssim 0.6$, and and CosmoDwarf, which has no disc structure at all, we take all particles within 0.1 virial radius into account. The 0.1 $R_{\rm vir}$ sphere is divided into shells with thicknesses set such that the number of particles within each shell is proportional to the square of the layer number counted from inside out. The total angular momentum of each shell is calculated and used to define the z direction of the corresponding shell. Each shell is then further divided into several annuli at different θ, with heights set such that the number of particles in each annulus is proportional to the corresponding $\sin\theta$ value. The average rotational velocity of each annulus is then subtracted. After this, each annulus is separated into cells containing roughly 15 particles. The dimensions of the cells are consistently set so that if all gas particles were distributed uniformly within the 0.1 $R_{\rm vir}$ sphere, each cell would be a cube with an identical volume. Within each cell, the average velocities in the $\hat{r}$, $\hat{\theta}$ and $\hat{\phi}$ directions are subtracted, and the particles with the highest 32% $|\mathbf{v} - \bar{\mathbf{v}}|^2$ are excluded. The turbulent kinetic energy is then calculated as the remaining kinetic energy.

To avoid biasing our comparison, we calculate the volume-integrated magnetic energy only for the gas particles in the same volume as in the turbulent energy calculation (without excluding any of them). The comparisons of the resulting turbulent energy and magnetic energy per unit mass are shown in Fig. 11. The turbulent kinetic energy grows almost immediately in these runs and quickly reaches a quasi-steady-state saturation level. With standard feedback, the turbulent energies per unit mass of Sbc, Mw and Ell all saturate to roughly $1 \times 10^{12} - 3 \times 10^{12}$ erg/g, corresponding to an rms turbulent velocity of $7 - 13$ km/s. HiZ on the other hand has slightly higher turbulent energy, $3 \times 10^{12} - 6 \times 10^{12}$ erg/g, corresponding to an rms turbulent velocity of $15 - 20$ km/s. Among all the runs, the SMC and CosmoDwarf runs have the lowest turbulent energy ($1 \times 10^{11} - 3 \times 10^{11}$ erg/g) and rms turbulent velocity

[3] For the HiZ runs, a cylinder with radius 35 kpc and height 10 kpc is used instead because its star-forming regions are spread over a significantly larger volume than in the other runs.

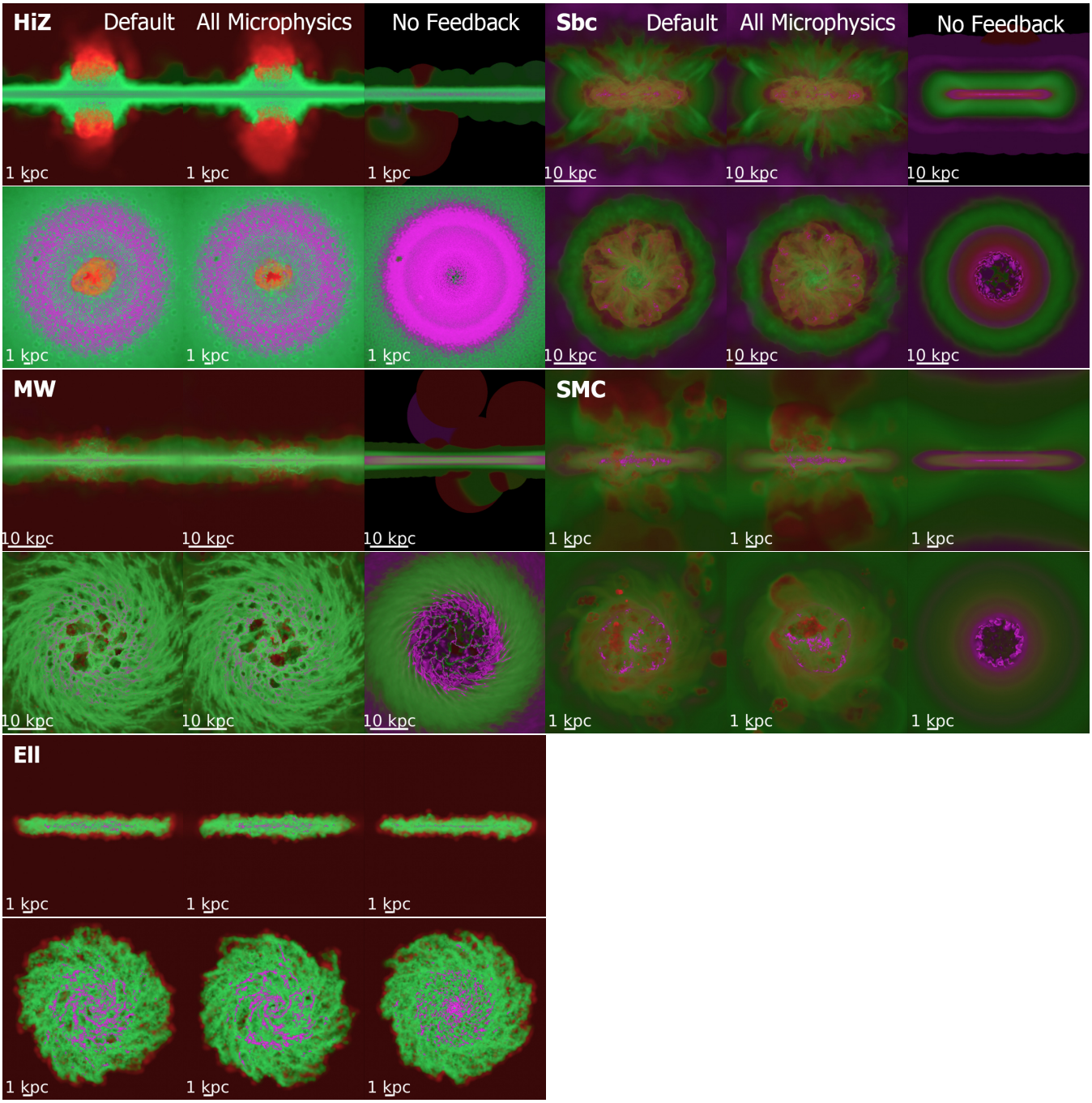

Figure 3. Images of the gas morphology of the isolated galaxies. The intensity encodes the projected density (log-weighted with ~ 4 dex stretch); different temperatures are shown in red ($> 10^5$ K), green ($8000 - 10^5$ K), and magenta (< 8000 K). We show edge-on and face-on projections for our default, all-microphysics (MHD is similar) and no-feedback runs. Without feedback, the gas collapses into high-density clumps and filaments at the galaxy centers, the discs are thin and lack galactic fountains, and hot gas is largely absent. However, the morphologies of the runs with the same stellar feedback but different additional physics show little difference. The SMC runs are more sensitive to stochastic SN events because of the lower galaxy mass (thus the images from runs with different microphysics can look slightly different at the same simulation time but are very similar on average). N.B.: The edge-on images for some of the no-feedback runs feature artifacts caused by the fact that there are very few gas particles above and below the disc.

(2-4 km/s), owing to this galaxy having a significantly lower mass and thus requiring less turbulent energy to self-regulate (Faucher-Giguère et al. 2013; Hayward & Hopkins 2015). The turbulent energy of CosmoMW at low redshift is calculated to be roughly the same as the values of HiZ, which is higher than the results from the isolated MW simulations. However, the turbulent energy at low redshift may be slightly over-predicted since all the particles within 0.1 virial radius are included for consistency even though a disk is already formed. If we include only the gas particles in the disk at low redshift, the turbulent energy drops to roughly $1 \times 10^{11} - 3 \times 10^{11}$ erg/g, similar to the results from the isolated MW simulations. Stellar feedback slightly boosts the turbulent energy, without which the

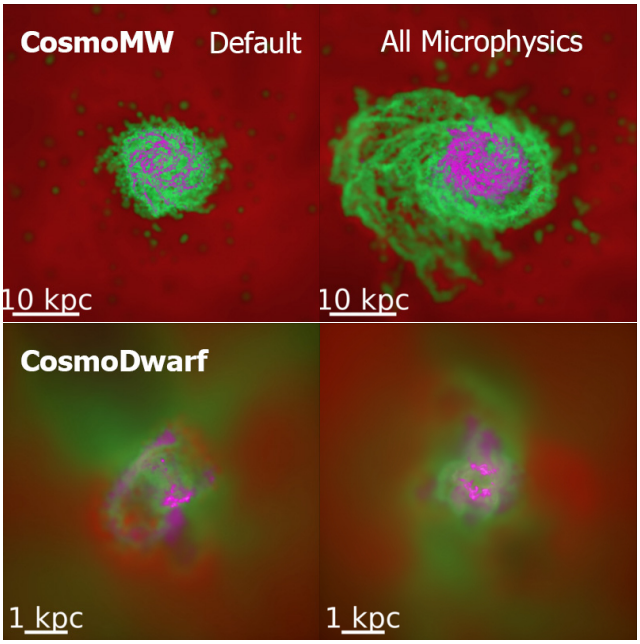

Figure 4. Images of the gas morphology of the cosmological simulations at $z = 0$, as Fig. 3. The slightly puffier disk in the CosmoMW all-microphysics run is likely to be a result of the stochastic variation in the merger history..

turbulent energy of each case drops by a factor of 3-10, and the rms turbulent velocity drops by a factor of $2-3$. The values we get are in good agreement with observations (Merrifield 1992; Levine et al. 2006) and the theoretical prediction that turbulent velocity for a marginally stable (turbulent $Q \sim 1$) disk is $\sigma_T \sim f_{\rm gas} v_c$, where v_c is the circular velocity, and $f_{\rm gas}$ is the ratio of the thin-disk gas mass to total enclosed mass in the galaxy (Faucher-Giguère et al. 2013; Hayward & Hopkins 2015).

As expected, we see that the magnetic energy grows from being negligible relative to the turbulent energy (because of the small initial seed fields used) until it saturates at $1\times10^{11}-5\times10^{11}$ erg/g in the HiZ, Sbc, MW and Ell runs and $\sim 10^{10}$ erg/g in the SMC and CosmoDwarf runs; these values are roughly 10% of the turbulent energy similar to values measured in idealized simulations of the super-sonic turbulent dynamics (Wang & Abel 2009; Dubois & Teyssier 2010; Kotarba et al. 2010). However, since (by construction) the initial field value is close to the equipartition value in the Ell run, the amplification is relatively mild in this case. Conduction, viscosity, and turbulent metal diffusion have little effect on the saturated field strengths. The corresponding rms magnetic fields are shown in Fig. 12, where the thick lines show the rms magnetic fields of all gas particles and the thin lines show the values of only the cold (< 8000K) gas. Although the total rms magnetic fields vary among different galaxy types because we use the same sampling volume for galaxies with different size, the rms magnetic fields of cold particles saturates to roughly 10 μG in all cases, in good agreement with both observations (Beck et al. 1996; Widrow 2002; Kulsrud & Zweibel 2008; Bernet et al. 2008; Kronberg et al. 2008; Jansson & Farrar 2012a,b) and other simulations (Wang & Abel 2009; Dubois & Teyssier 2010; Kotarba et al. 2010, 2011; Beck et al. 2012; Pakmor & Springel 2013).

The direct comparison of magnetic and turbulent energy clearly illustrates that the turbulence is both super-Alfvénic and super-sonic. In this limit, we expect magnetic fields to have a negligible effect on the turbulent kinetic energy and only a weak effect on the density fluctuations driven by turbulence (Molina et al. 2012; Federrath et al. 2008, 2011; Kainulainen & Tan 2013). In contrast, for typical magnetic field strengths, the turbulent velocities of the runs without feedback have Alfvénic Mach numbers of order unity; in this case, magnetic fields have a strong back-reaction on the turbulent flow, and the turbulence is therefore no longer isotropic (Molina et al. 2012). This partially explain why magnetic fields have been observed to have strong effects in other studies where stellar feedback is absent or weak but not in ours.

4.5 Galactic outflows

In simulations that explicitly include multiple stellar feedback channels, such as those presented in this work, strong outflows are generated self-consistently. We quantify the outflow phase structure in Fig. 8-10 and gas velocity distribution in Fig. 13. Detailed analyses of these properties using similar simulations with the same physics as our "default" case are presented in Hopkins et al. (2012a, 2013b) (for isolated galaxies) and in Muratov et al. (2015) (for cosmological simulations); here, our focus is only on how the outflow properties depend on the included microphysics.

Fig. 13 and Fig. 14 plot the distribution of the radial velocities (defined relative to the baryonic center-of-mass of the galaxy) of gas particles within the same volume as stated in § 4.4[4] averaged over the entire simulation duration (or appropriate redshift ranges for the cosmological runs). To isolate "outflows" in Fig. 8-10, we simply take all gas particles within a thin layer at the boundary of the galaxy region defined above that have a radial velocity greater than some $v_{\rm min}$ chosen to be an appreciable fraction of the escape velocity of each galaxy ($v_{\rm min} = 200$, 100, 100, 30, 100, 100, and $30\,{\rm km\,s^{-1}}$ for the HiZ, Sbc, MW, SMC, Ell, CosmoMW and CosmoDwarf runs, respectively).

Galactic outflows only exist when there is feedback, while MHD and the additional physics that we study appear to have little effect on the velocity or density of the outflows.

5 DISCUSSION: WHY ARE THE EFFECTS OF THE ADDITIONAL MICROPHYSICS WEAK?

We have seen systematically that for the large-scale properties of star formation, ISM structure, and galactic outflows, magnetic fields and microphysical diffusion processes make little difference once explicit stellar feedback is included. Here we discuss why this is the case.

5.1 Sub-grid metal diffusion

The microscopic (Brownian) diffusivity of metals is negligibly small for the systems we simulate. Instead, Smagorinski-type (mixing length theory) models assume that unresolved turbulent eddies can be treated as a scale-dependent diffusion process with diffusivity $\sim v_t(\lambda)\,\lambda$ (where $v_t(\lambda)$ is the rms turbulent velocity measured on length scale λ). The "sub-grid" part of the model applies an explicit extra diffusion term using $\lambda \rightarrow \Delta x$ (where Δx is the spatial resolution) to account for un-resolved eddies, with the assumption that all larger eddies are resolved and that the $v_t(\Delta x)$ measured around each point is indeed turbulent motion. But for

[4] For CosmoMW, unlike in § 4.4, in which the same sampling volume is used for all redshifts, we switch to a cylinder with radius 10 kpc and height 2 kpc at low redshift because it better captures the wind properties at the time when a disc has already formed.

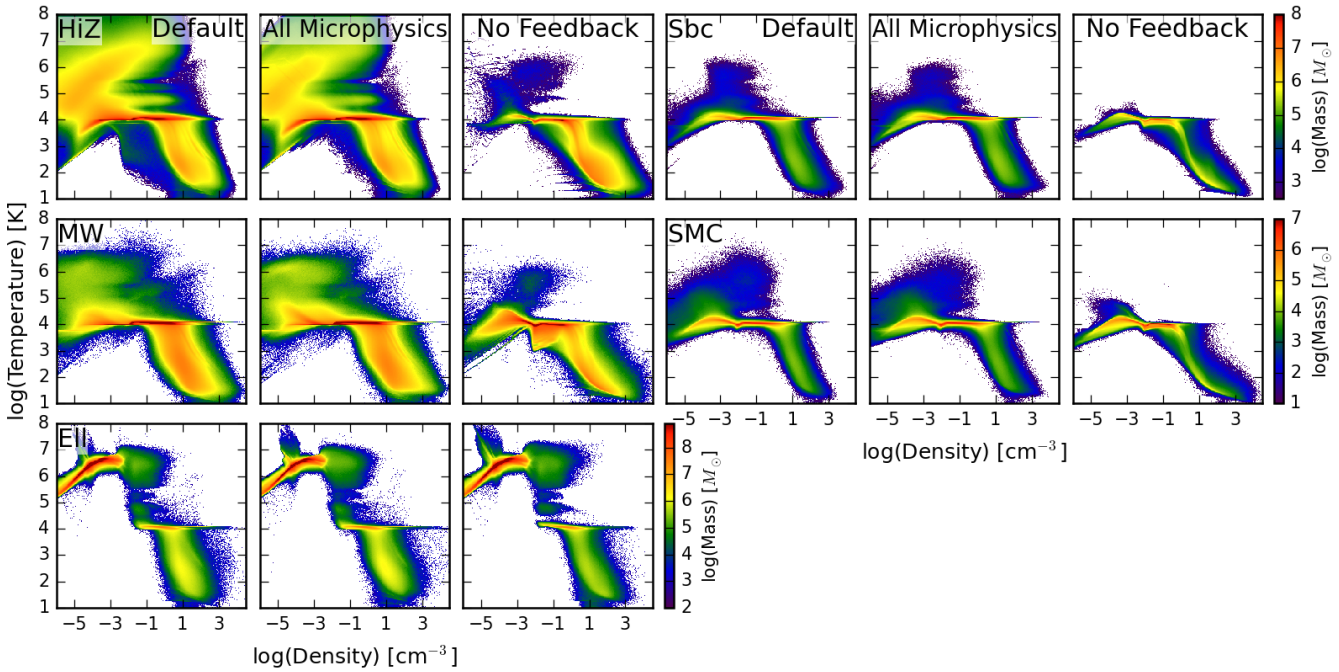

Figure 5. Temperature-density phase distribution of our isolated galaxy simulations. Each plot is averaged over the entire simulation duration. With feedback, cold neutral, warm ionized, and hot (feedback-driven) volume-filling phases are present. Absent feedback, more cold gas appears owing to rapid collapse, and it is colder owing to the lack of local photo-electric heating; HII-region ($T \sim 10^4$ K and high-density) gas is absent; and almost no hot gas is present (except in the Ell run, where the hot gas is dominated by the initial hot halo – even here, however, the hot gas ejected by the disc is dramatically suppressed). The additional MHD and diffusion microphysics have little effect on the phase structure in the presence of feedback. Note that the "spike" in the upper-left corners (hot halo phase) of the Ell runs correspond to an artificial shock arising from the IC being out of equilibrium.

a super-sonic cascade, or any system obeying the observed line width-size relation (which we have demonstrated is satisfied by our simulations with stellar feedback in Hopkins et al. 2012b), $v_t(\lambda)\,\lambda \sim (G\Sigma\pi)^{1/2}\lambda^{3/2}$, where Σ is the surface density. Thus, the power and diffusivity is concentrated in the largest-scale eddies. In the disc, these have scales of order the disc scale height; in the halo, the relevant scales are a large fraction of the halo core radius. In either case, the largest-scale eddies are well-resolved. In fact, taking the resolved line width-size relations found in our previous work (Hopkins et al. 2012b) and integrating (assuming an infinite inertial range), we expect that most of the global diffusivity is resolved. Thus, the only effect of the sub-grid diffusivity is to smooth particle-to-particle variations in metallicity after bulk mixing of the metals (by particle motion) is resolved. In principle, this can alter the cooling rates, but the effect is weak because the resolution is high enough that we account for individual SNe explosions (so that the Poisson noise in the number of enrichment events that each particle sees is small; Ma et al. 2015; van de Voort et al. 2015). Although subtle effects, e.g. the predicted dispersion in abundances within star clusters, may not be well captured by our simulations, these have little effect on the global properties that we focus on herein.

To the extent that much larger effects are found using similar mixing models (Shen et al. 2010; Wiersma et al. 2009b), one of three effects is likely to be occurring in those works. (1) The turbulent driving scales are not resolved (so there is little or no resolved mixing). This is certainly the case in simulations with force softening $\gtrsim 100$ pc. However, in this case, it is not correct to apply the Smagorinski model in its typical form, since (as discussed above) it explicitly assumes that all shear motion in the simulation around a particle is resolved turbulent motion (from which it extrapolates the inertial range). (2) Additional motions (e.g. orbital motions in a disc or outflow motions in winds) are accidentally triggering the numerical "turbulent velocity" estimator. This effect is also likely to be more severe in lower-resolution simulations but is a serious concern when sub-grid diffusion models are applied to galaxy simulations at any resolution. (3) The coefficient of the diffusivity is too large (or the numerical gradient estimator is inaccurate), so the diffusivity assigned to un-resolved eddies can be larger than that of larger, resolved eddies. This can easily occur if $C \gtrsim 1$ is used, or if the gradient estimator is noisy (which is commonly the case in SPH).

5.2 Conduction & viscosity

We can also understand why physical conduction and viscosity have weak effects in the simulations presented in this work. Like all numerical methods, our Godunov-type solver has inherent numerical diffusion, with a numerical diffusivity that scales (crudely) as $\sim c_s\,\Delta x$ (where Δx is the spatial resolution). Comparing this to Spitzer-Braginskii conduction (diffusivity $\sim (\kappa\, m_p)/(k_B\,\rho)$), and using the fact that our code is Lagrangian (so $\rho \sim m_i/\Delta x^3$, where m_i is the particle mass), we estimate that physical conductivity dominates our numerical when $T \gtrsim 0.3\times10^7\,\mathrm{K}\,(m_i/10^4\,M_\odot)^{1/6}\,(n/0.01\,\mathrm{cm^{-3}})^{1/3}$. Moreover, as mentioned in § 5.1, large-scale turbulent eddies have diffusivity $\sim v_t(\lambda)\,\lambda \sim (G\Sigma\pi)^{1/2}\lambda^{3/2}$. We estimate the micro-physical conductivity to surpass this turbulent value at an even higher temperature $T \gtrsim 3\times10^7\mathrm{K}(\Sigma/(100 M_\odot pc^{-2}))^{3/5}(\lambda/100pc)^{1/5}$. Thus, only in the hot, tenuous gas phase can physical conductivity be significant relative to the turbulent (and numerical) diffusivity.

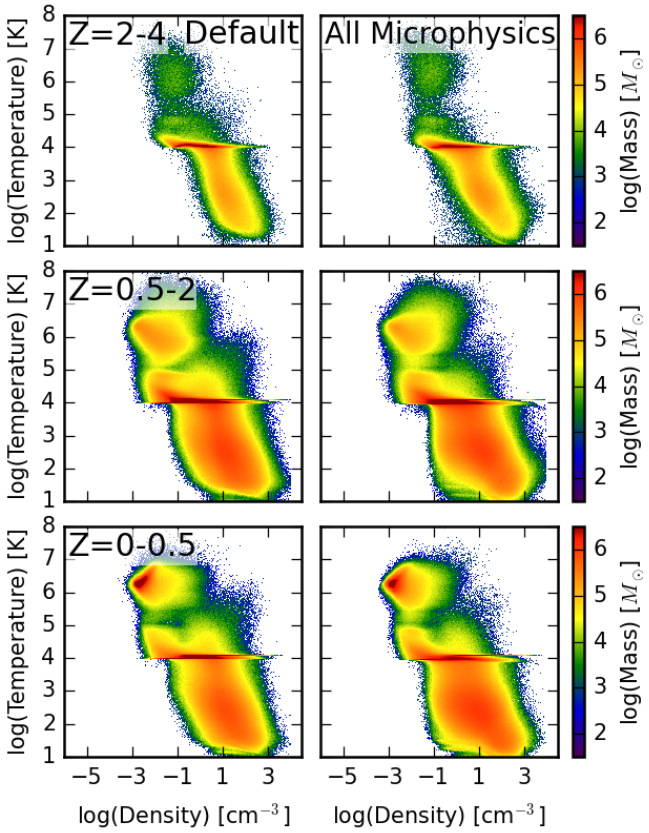

Figure 6. Temperature-density phase distribution of the CosmoMW cosmological simulation. Each plot is averaged in three separate redshift intervals (labeled). With feedback, cold neutral, warm ionized, and hot (feedback-driven) volume-filling phases are present. The additional MHD and diffusion microphysics have little effect in the presence of feedback.

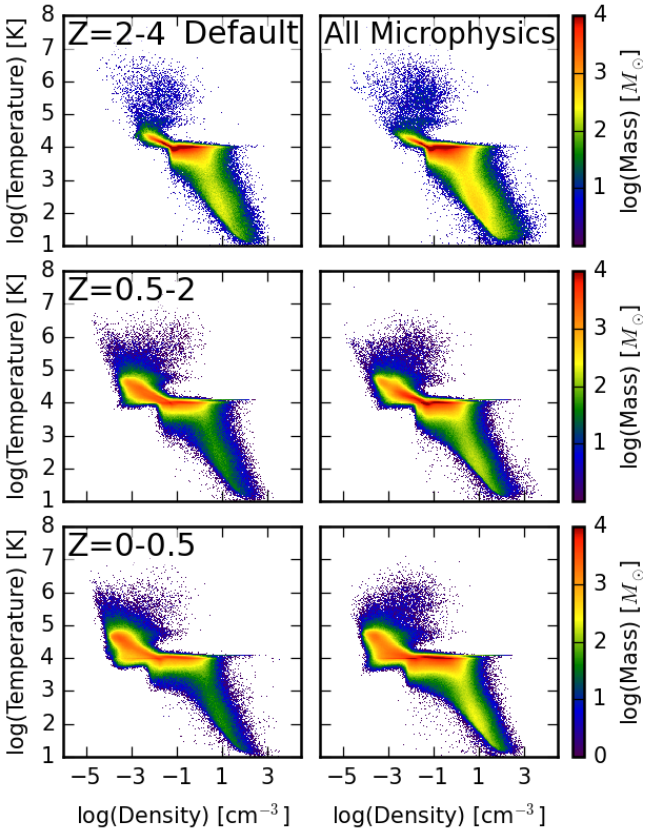

Figure 7. Temperature-density phase distribution of our CosmoDwarf cosmological simulation. Each plot is averaged in three separate redshift intervals (labeled). With feedback, cold neutral, warm ionized, and hot (feedback-driven) volume-filling phases are present. The all-microphysics run has slightly more cold neutral gas than the other runs.

Even under these conditions, however, the conduction timescale is generally longer than the characteristic cooling and/or dynamical times: the Field length (the characteristic scale below which conduction is faster than cooling) is $\sim [(\kappa\, m_p\, t_{\rm cool})/(k_B\, \rho)]^{1/2} \sim {\rm pc}\,(T/10^7\,{\rm K})^{7/4}\,(n/0.01\,{\rm cm}^{-3})^{-1}$. In our simulations, the Field length is typically much smaller than the resolved scales of structures (including coherent filaments and dense gas blobs). This indicates that while conduction and viscosity may have interesting effects on small scales, explicitly including them in galaxy simulations at present is not expected to have a large impact. This does not, of course, guarantee that conduction and viscosity cannot have effects that feed back to large scales in fully resolved simulations. More work will be needed to answer this latter question.

The only exception, where conduction and viscosity generate a small, but visible systematic effect is the CosmoDwarf case, in which the all-microphysics run has ~ 0.2 dex higher stellar mass and cold gas mass and more stable SFR and cold clumps. These are most likely caused by conduction. In a dwarf galaxy of this mass, an overlap of SNe can easily wipe out all the cold gas in the galaxy, which happens several times throughout the simulations. However, conduction could dissipate part of the SNe energy, making it more difficult for them to completely destroy the cold clumps in the ISM. From the star formation histories, we infer that a typical event capable of "wiping out" all the cold gas requires an overlap of ~ 100 SNe. To show that conduction can actually be effective in this limit, we can compare the time scale of energy dissipation by conduction, $\tau_c \equiv E/\dot{E}_{\rm conduction}$, to the free expansion time of SNe in the energy conserving phase, $\tau_{\rm exp} \equiv R/v$, where $E = N_{\rm SNe}10^{51}$ erg is the energy sum of the $N_{\rm SNe}$ overlapping SNe, R is the radius of the expanding hot bubble and v is the speed of expansion. $\tau_c/\tau_{\rm exp}$ turns out to be $\sim 6\times10^{-6}(R/10pc)^7(N_{\rm SNe}/100)^{-2}(n/cm^{-3})^3 < 1$, which means conduction cannot be neglected. As the expansion continues, the radius grows, $\tau_c/\tau_{\rm exp}$ drops and the importance of conduction gradually decays. However, before conduction ceases to be important ($\tau_c/\tau_{\rm exp} = 1$), the hot bubble can entrain a total mass of $\sim 10^4(N_{\rm SNe}/100)^{6/7}(n/cm^{-3})^{-2/7}M_\odot$, which is well resolved in our CosmoDwarf simulations. The effects of conduction are therefore expected to be visible in our CosmoDwarf simulations, where the resolution is high enough and the size small enough for the cold gas to be mixed in overlapping SNe remnants.

5.3 Magnetic fields

We can also understand in simple terms why magnetic fields have little effect on the galaxy SFRs and, consequently, their position in the Schmidt-Kennicutt diagram and other SF scaling laws. In a series of previous studies (Hopkins et al. 2011, 2012b, 2013a,d,c; Faucher-Giguère et al. 2013; Hopkins et al. 2014), we have repeatedly shown that galaxy SFRs are set by a balance between stellar feedback injecting momentum ("resisting" collapse and the"stirring" of super-sonic turbulence) and dissipation of that mo-

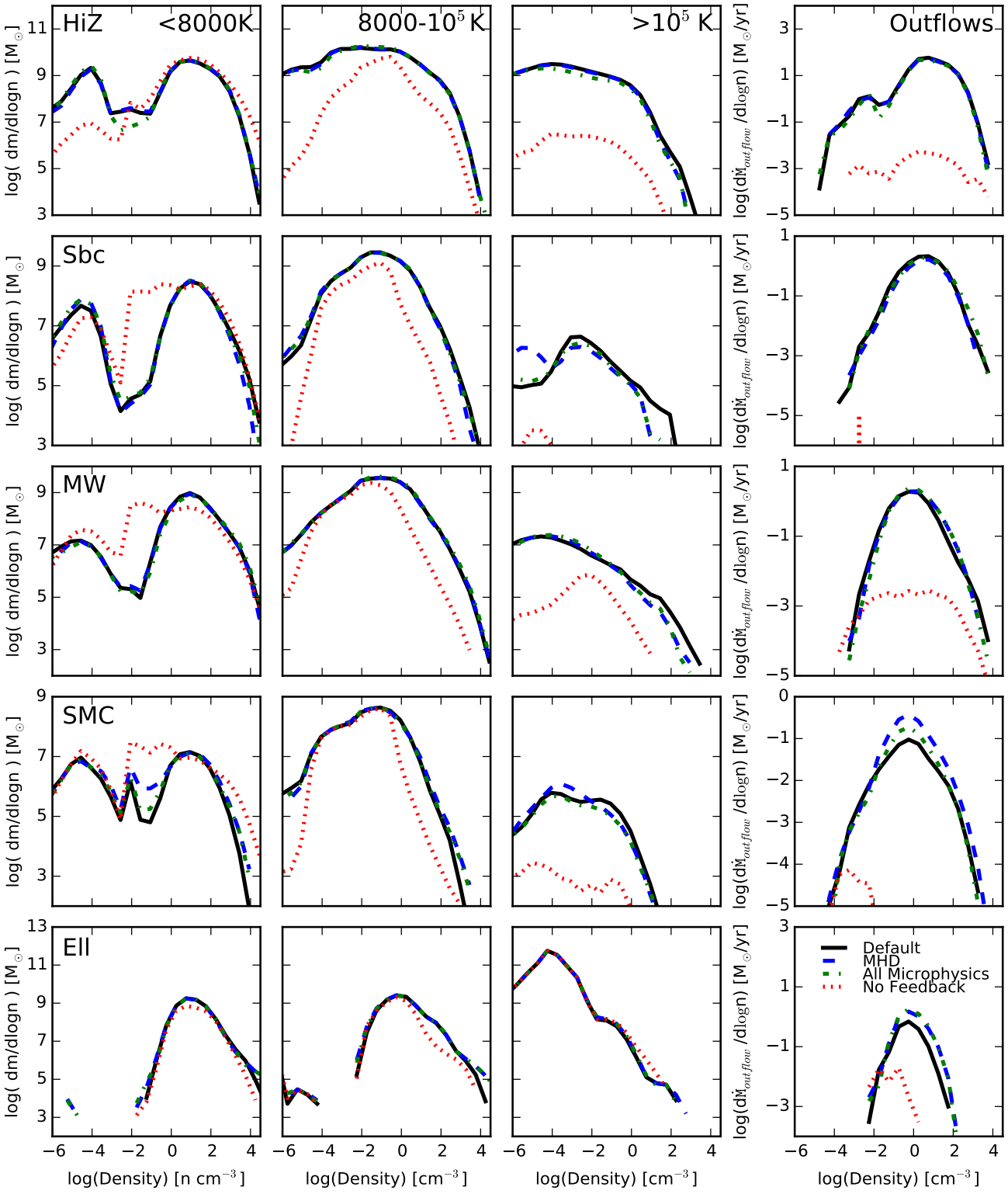

Figure 8. Density distribution of gas in different phases. Rows show our isolated galaxy simulations; columns show phases including cold neutral (*left*), warm ionized (*middle left*), hot (*middle right*), and outflow (*right*). To estimate the outflow, we simply take all gas that is within 0.5 kpc of the boundary of the disc (taken as a cylinder with radius 10 kpc and height 2 kpc) and moving with a radial velocity greater than some $v_{\rm min}$ chosen to be an appreciable fraction of the escape velocity in each galaxy ($v_{\rm min} = (200,\ 100,\ 100,\ 30,\ 100)\,{\rm km\,s^{-1}}$ for HiZ, Sbc, MW, SMC, and Ell runs, respectively). The no-feedback runs produce far less outflow and hot gas, and more cold gas, as expected (the difference is again less visible in the Ell run since the hot phase is dominated by the initial hot halo gas). Varying the additional microphysics has relatively weak effects.

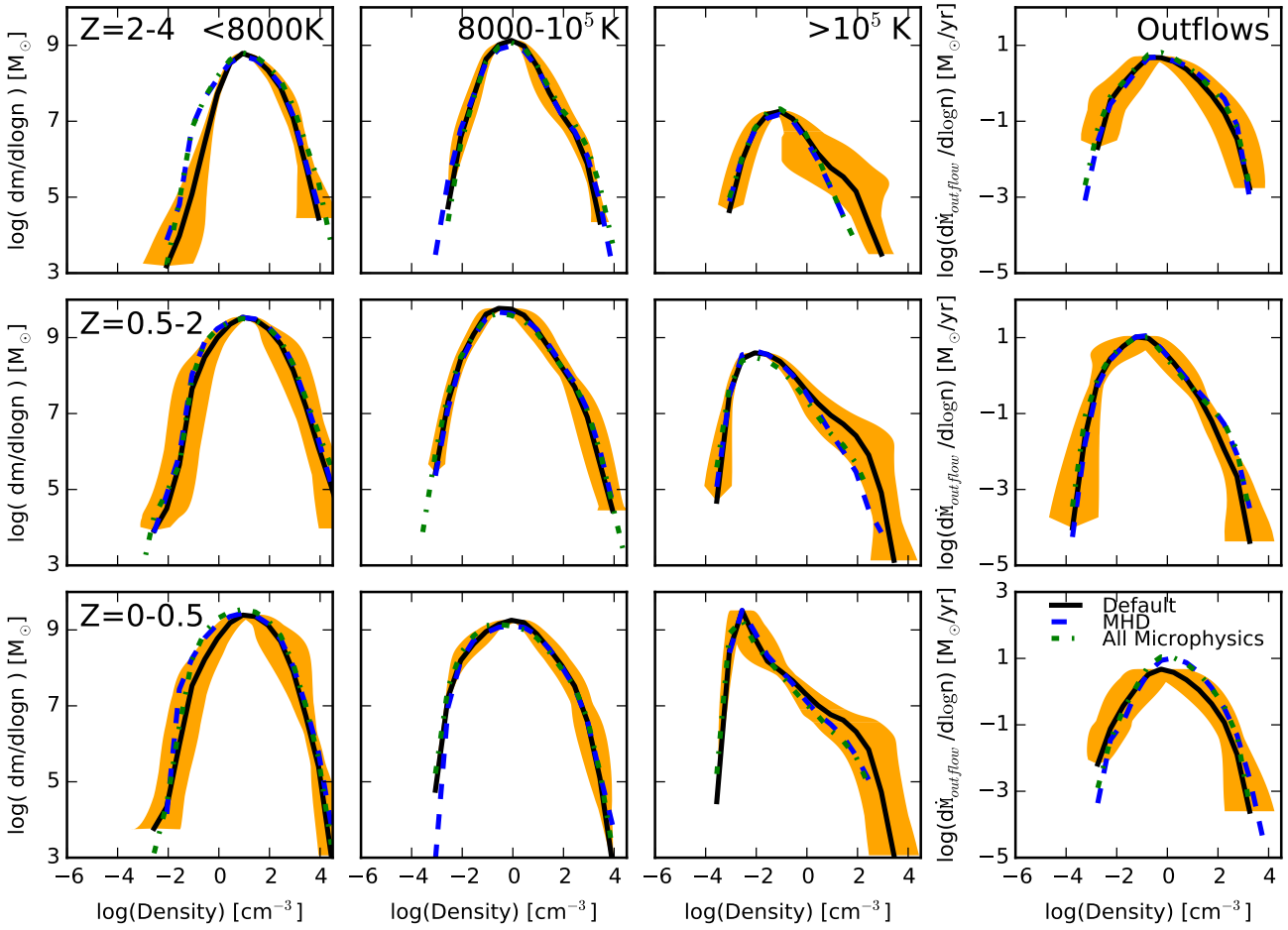

Figure 9. Gas density distribution in different phases, as in Fig. 8, but for our CosmoMW run, averaged in different redshift intervals. To quantify the outflows for at $z = 0.5 - 4$, instead of using a disc, we select all gas located between 0.08 and 0.1 virial radii of the halo center that is moving with a radial velocity greater than $100\,\mathrm{km\,s^{-1}}$. The orange shaded regions in each panel indicate the magnitude of stochastic effects (see text for details). At each redshift, the properties are similar in all runs with stellar feedback.

tion via gravitational collapse. Other groups have reached consistent conclusions in calculations that include self-gravity, resolve fragmentation and turbulence, and explicitly model stellar feedback (Shetty & Ostriker 2008; Agertz et al. 2013; Kim et al. 2013, 2014). In such simulations, galactic SFRs are independent of the sub-grid model for how dense gas turns into stars (Hopkins et al. 2011, 2013d), the shape and orders-of-magnitude variation in the cooling function and modeled dense gas chemistry (Hopkins et al. 2012b), and the temperature and detailed kinematics of the star-forming gas (Hopkins et al. 2013c). Even equipartition magnetic fields would only change the equilibrium SFR in this scenario by only tens of percent. Similar arguments apply to galactic outflows: the mass outflow rate is set by the momentum injected by feedback, which is divided into stirring turbulence in the disc and ejecting low-density material (Murray et al. 2011; Thompson & Krumholz 2014; Hayward & Hopkins 2015; Martizzi et al. 2016), and ultimately limited by the depth of the potential (Muratov et al. 2015). We thus do not expect the mass outflow rate to vary by large factors when magnetic fields are present.

Perhaps the most surprising result of this study is how weak the effects of magnetic fields are on the ISM phase structure. Using the same code in idealized tests, we have shown that sufficiently strong magnetic fields do produce qualitatively different behavior in fluid mixing instabilities, cloud entrainment or "crushing" by ambient winds, and anisotropic super-sonic turbulence (Hopkins & Raives 2016), in agreement with a vast literature. Moreover, the rms fields we predict in both ambient gas and dense clouds are in reasonable agreement with those observed, as discussed in § 4.4. However, it appears that two main effects lead to relatively weak effects of magnetic fields on the large-scale phase structures we consider. (1) The turbulence in most of the disc is super-Alfvénic, at least on large scales that contain most of the power (size of the disc scale height, also corresponding to the size of the largest GMCs, which contain most of the dense gas mass and star formation). Thus, the turbulent velocity dispersions, isotropy, and density fluctuations generated are not strongly altered (Molina et al. 2012; Federrath et al. 2008, 2011; Kainulainen & Tan 2013). (2) GMCs are not steady-state, pressure-confined, equilibrium objects in the simulations. We have previously shown (Hopkins et al. 2012b) that in similar simulations, GMCs form rapidly (in a single dynamical time) from gravitational instability (and are self-gravitating) and

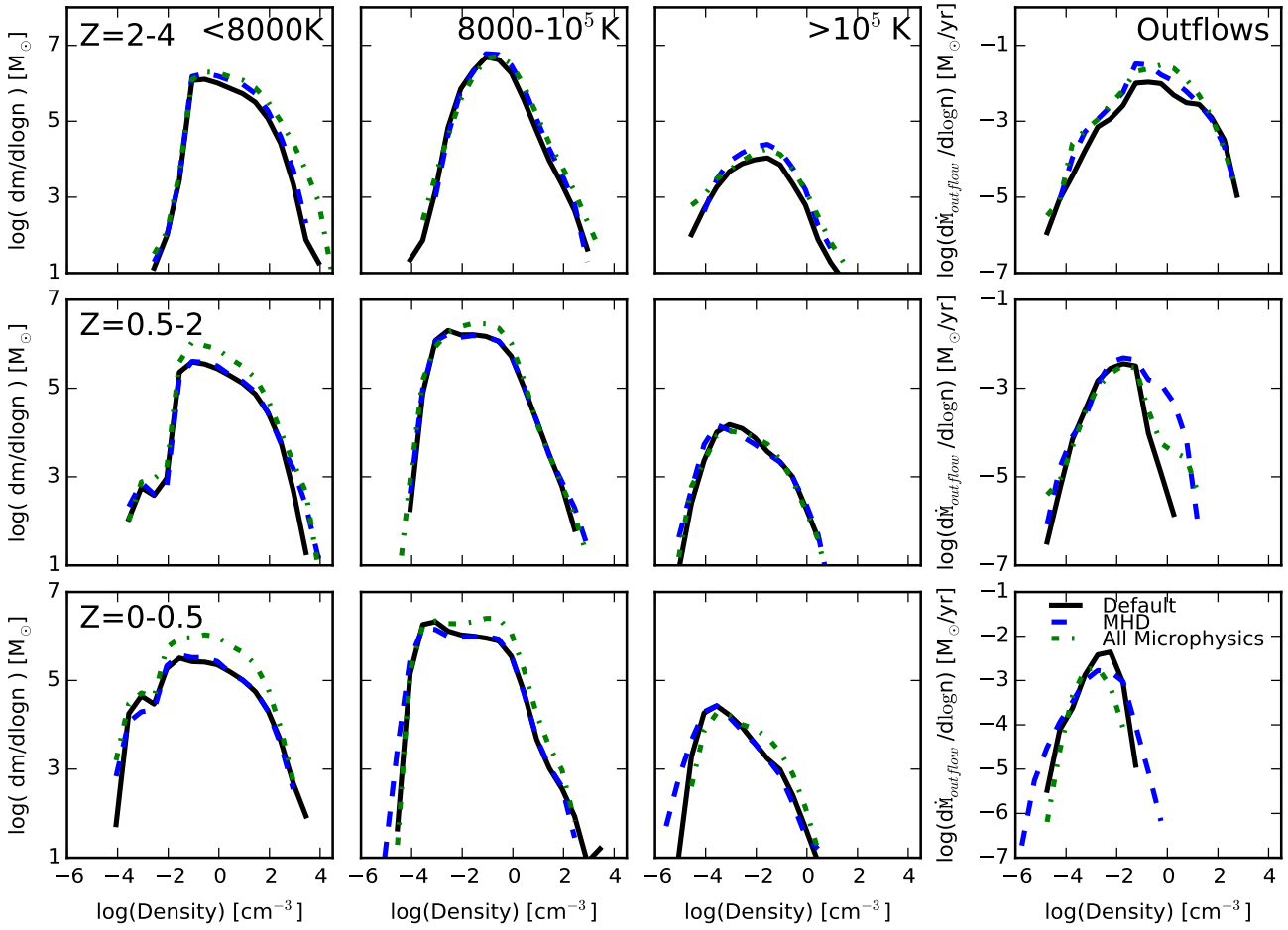

Figure 10. Gas density distribution in different phases, as in Fig. 8, but for our CosmoDwarf run, averaged in different redshift intervals. To quantify the outflows, instead of using a disc, we select all gas located between 0.08 and 0.1 virial radii of the halo center that is moving with a radial velocity greater than $30\,\mathrm{km\,s^{-1}}$. At each redshift, there is slightly more cold gas in the all-microphysics run, consistent with the slightly higher stellar mass and more stable cold clumps. There is a hint of more high-density outflow material in the MHD run, but this appears to vanish when the additional microphysics is added.

live just a few dynamical times, forming stars via turbulent fragmentation until feedback disrupts the cloud.

McCourt et al. (2015) recently showed that magnetized gas clouds can survive much longer than unmagnetized ones when accelerated by supersonic hot wind. Our simulations suggest that magnetic fields play a less important role in the formation and survival of dense cold clouds in the ISM of galaxies, such as molecular clouds. One important difference is that massive molecular clouds are typically self-gravitating, rather than in pressure equilibrium with the surrounding ISM. Moreover, as explained above, in our simulations, massive molecular clouds are disrupted by stellar feedback rather than by hydrodynamic instabilities. As for the cold clouds in the outflow, although our simulations also suggests little importance of magnetic field, we caution that the only 2 galaxies in our study with "hot halos" are Ell and CosmoMW. In our other simulations, such cloud "shredding" or mixing effect will be much weaker since there is little or no hot gas halo for the cold outflow gas to mix into. In the Ell and CosmoMW cases where there are hot halos, the achievable resolutions are inevitably lower, meaning the phase structure in the outflows may not fully resolved. Besides, most of the outflow mass which reaches large radii ($\gtrsim R_{vir}$) is hot gas in the first place - cold outflows tend to be recycled in small-scale fountains (see Muratov et al. 2015).

Despite the weak role that magnetic fields play, we see a hint of a small (< 0.1 dex) increase of stellar mass in those runs with magnetic fields. Interestingly, magnetic fields may, if anything, enhance star formation on large scales. The fact that the difference is more obvious in the smaller galaxy suggests that this may result from magnetic field helping stabilizing colds clumps in the ISM, especially in the small galaxies with less stable cold phase.

6 CONCLUSIONS

We use simulations with parsec-scale resolution, explicit treatments of stellar feedback identical to those used in the FIRE project, magnetic fields, anisotropic Spitzer-Braginskii conduction and viscosity, and sub-grid turbulent metal diffusion to study how these affect galaxy-scale star formation, the phase structure of the ISM, and the generation of galactic outflows. We consider both isolated (non-cosmological) simulations of a range of galaxy types and fully cosmological zoom-in simulations of a Milky Way-mass halo and a dwarf halo.

In all cases, we find the following:

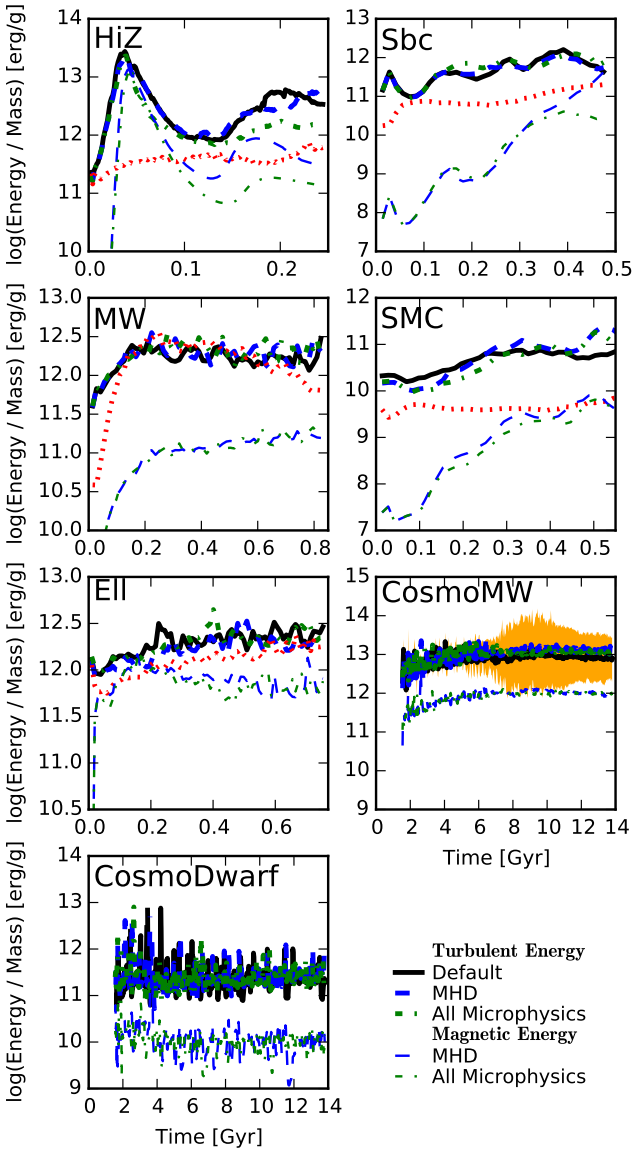

Figure 11. The total turbulent kinetic energy (*thick lines*; defined in § 4.4) and magnetic energy (*thin lines*) per unit mass of the non-outflowing disc gas in our simulations is shown as a function of time. In the CosmoMW case, the orange shaded region shows the magnitude of stochastic effects on the turbulent energy. In all cases, the turbulent energy saturates at a steady-state value over many dynamical times, corresponding to supersonic and super-Alfvénic velocity dispersions. The steady-state value is only very weakly altered by MHD and microphysical diffusion, consistent with expectations for super-Alfvénic turbulence on large (galactic) scales. The magnetic energy grows from the seed value to $\sim 10\%$ of the turbulent kinetic energy, consistent with idealized simulations of the supersonic turbulent dynamo. "No feedback" runs produce noticeably weaker turbulence (although *local* bulk motions from collapsing structures can be large, they are excluded by our estimator), suggesting stellar feedback is critical to maintain the turbulent cascade.

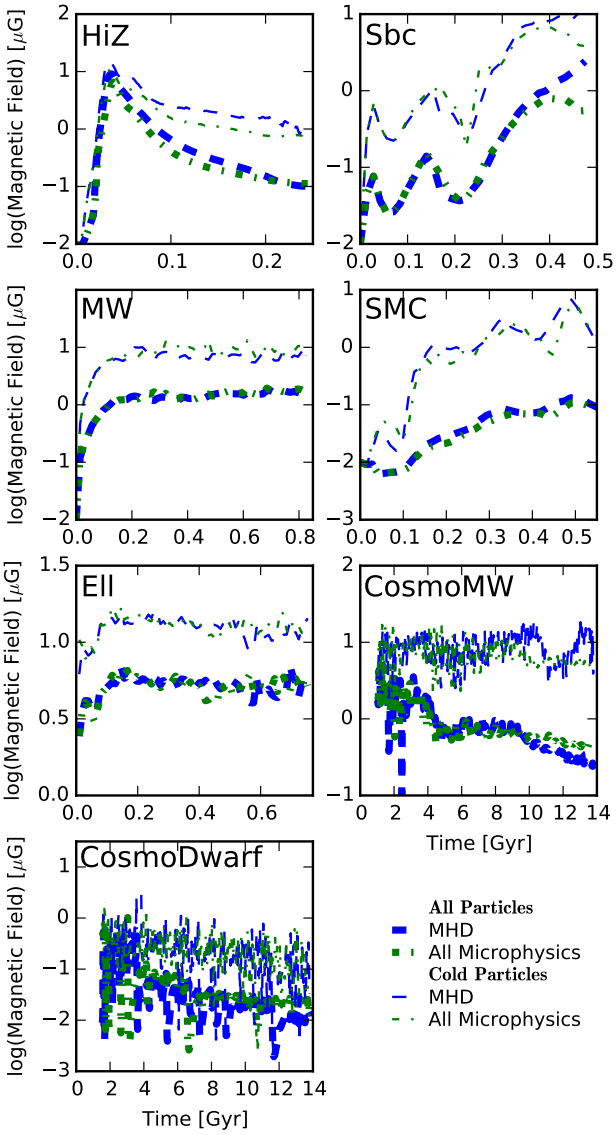

Figure 12. The rms magnetic field strength of all (*thick lines*) and the $T < 8000$ K component (*thin lines*) of the non-outflowing disc gas in our simulations is shown as a function of time. The magnetic field is amplified from the seed value to $\sim 1 - 10$ μG. Although the average value over all particles varies among different galaxies, the rms magnetic field strength of cold gas saturates at several to 10 μG, consistent with observations and other simulations.

• Stellar feedback plays the dominant role in regulating the SFR. Without feedback, the SFR is approximately the gas mass divided by the dynamical time, a factor of $\sim 50 - 100$ larger than observed. As shown in Fig. 1 and our previous studies (see the references in § 5.3), stellar feedback, when implemented explicitly following stellar evolution models and without fine-tuning, reduces the SFR by this factor and brings it into good agreement with the observed KS law and observed cosmological galaxy star formation histories. We find that once feedback is present, magnetic fields and additional microphysical diffusion processes change the SFR (and therefore the KS law) by small amount. This is consistent with the models advocated in the aforementioned papers, in which the

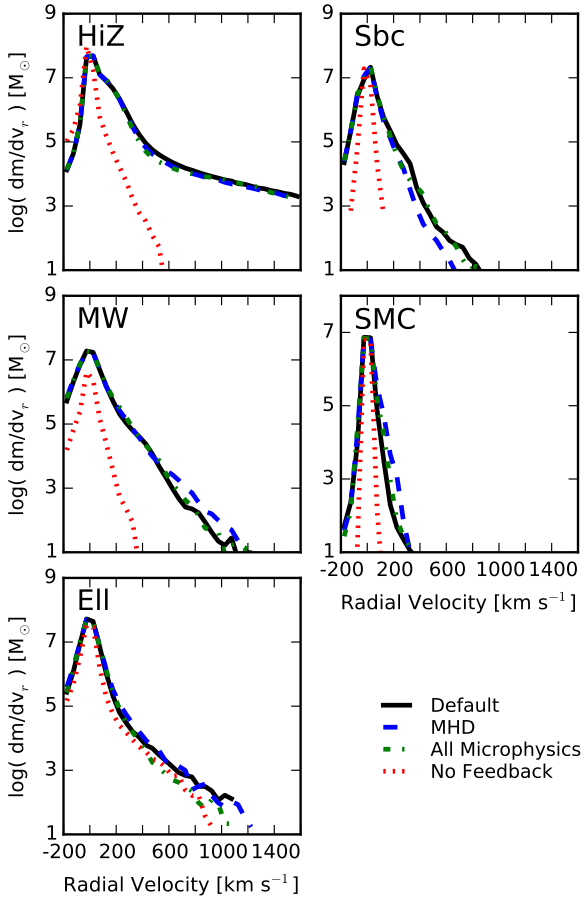

Figure 13. Distributions of the radial velocities of the gas particles in the isolated galaxy simulations. For each, we plot the time-averaged distribution of mass as a function of the radial velocity v_r with respect to the galaxy center of mass. Without feedback, there are essentially no outflows, and we see only turbulence and bulk non-radial motions inside the galaxies. Once stellar feedback is included, outflows are self-consistently driven (i.e. there are substantially more particles with large radial velocities). As long as stellar feedback is included, the velocity distribution function is insensitive to the microphysics investigated here.

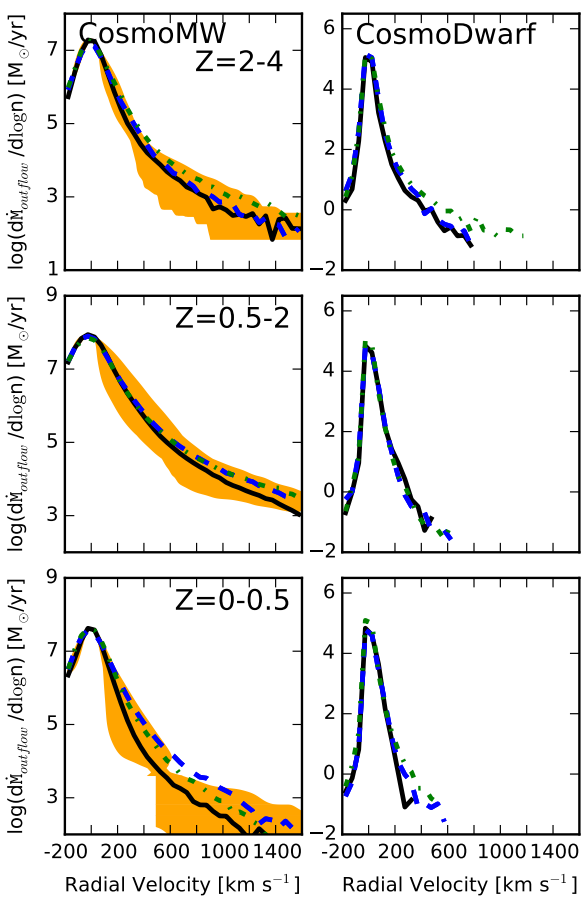

Figure 14. Distributions of the radial velocities of the gas particles in the cosmological simulations. For each, we plot the time-averaged distribution of mass as a function of the radial velocity v_r with respect to the galaxy center of mass. The orange shaded regions in the CosmoMW panels represent the magnitude of stochastic effects. With feedback included, outflows are self-consistently driven. The velocity distribution function is insensitive to the microphysics investigated here.

SFR and star formation scaling relations are set by self-regulation via feedback, which drives super-sonic turbulence and balances the disc against gravity.

- The ISM phase structure is also primarily stellar feedback regulated. With stellar feedback included, a multi-phase turbulent ISM with a physically reasonable morphology is established and maintained; our previous studies suggest that the properties of the simulated ISM agree well with observations (Hopkins et al. 2012b). In contrast, without feedback, gas experiences runaway collapse, producing discs with artificially small scale heights, excessive amounts of cold gas in dense clumps, and essentially no hot volume-filling gas (see Fig. 3, 5, 6, 8, 9). Similarly, stellar feedback drives energetic galactic winds, which are not present without feedback (Fig. 13). Stellar feedback also serves as an extra source of turbulent energy, boosting the rms turbulent velocity by a factor of 2-3. Perhaps surprisingly, however, neither MHD nor the additional diffusion microphysics appear to produce larger than $\sim$ 10%-level systematic effects on these quantities. In fact, in some earlier experiments where we artificially increased the viscosity coefficient η by a factor of 100, there were still weak systematic effects. It appears that because the turbulence is super-Alfvénic on the scales most important for fragmentation, ISM phase structure and outflow generation (of order the disc scale height), these effects are sub-dominant. A more detailed discussion of why such small effects are seen is provided in § 5.
- The magnetic field energies saturate at $\sim$ 10% of the turbulent kinetic energies on of order the galactic scale height (Fig. 11). The ratio is smaller still if we include the kinetic energy of small-scale galactic fountains in the "turbulence" budget. This is consistent with both observations (Beck et al. 1996; Widrow 2002; Kulsrud & Zweibel 2008; Bernet et al. 2008; Kronberg et al. 2008; Jansson & Farrar 2012a,b) and other simulations (Beck et al. 2012; Pakmor & Springel 2013; Wang & Abel 2009; Dubois & Teyssier 2010; Kotarba et al. 2010, 2011). This result partially explains why the magnetic field's effects are sub-dominant on the large scales of order the disc scale height (the scales containing most of the turbulent energy).
- A systemic increase of stellar mass and cold gas is observed in CosmoDwarf run with all fluid microphysics included. This may result from conduction dissipating part of the SNe energy making it

more difficult to wipe out cold clumps. A more detailed discussion of this is provided in § 5.

It appears that, at least on galactic scales, in the presence of explicit models for multi-mechanism stellar feedback as well as self-gravity, magnetic fields and additional diffusion microphysics (such as conduction, viscosity, and small-scale metal diffusion) are subdominant in the star formation and galaxy formation process at currently achievable resolutions. This general result appears to contradict some earlier claims in the literature. However, to our knowledge, these prior studies have not focused on the combination of large galactic scales (yet with high enough resolution to resolve vertical disc scale heights and the phase structure in discs) and fully explicit models for stellar feedback. For example, it is relatively "easy" for magnetic fields to have a large fractional effect in simulations with either no or weak stellar feedback or stellar feedback modeled only in a "sub-grid" fashion (so it e.g. does not locally alter the gas dynamics but only ejects gas in outflows or adds an effective pressure term). However, the claimed effects in these cases are typically order-unity (Piontek & Ostriker 2005, 2007; Wang & Abel 2009; Beck et al. 2012; Pakmor & Springel 2013) and thus still orders of magnitude less than the factor $\sim 100-1000$ changes in the properties we study here that occur when the full model for stellar feedback is introduced.

Altogether, our results support the emerging picture wherein galaxy-scale ($\gtrsim 10-100\,$pc) star formation, ISM structure, and outflows are determined primarily by a competition among supersonic (and super-Alfvénic) turbulence, stellar feedback, and self-gravity. The microphysics we study here may certainly be important on smaller scales (e.g. for regulating the structure of turbulent cores as they collapse to form stars) or in the more diffuse IGM (e.g. the outskirts of galaxy clusters). However, they do not, to leading order, significantly alter the dynamics on the scales we study here.

Although the magnetic field has little effect on the properties analyzed in our current study, it might for instance provide important pressure support in the violent tidal compression that occurs in galaxy mergers, which could possibly affect the properties of the star clusters formed in merger-induced starbursts. Besides stellar feedback and fluid microphysics, AGN feedback and cosmic rays are thought to be important physical properties, especially in the evolution of massive galaxies. Detailed investigations of these processes in the context of simulations with explicit stellar feedback will be presented in future work.

ACKNOWLEDGEMENTS

We thank Ai-Lei Sun, Shu-heng Shao, Eliot Quataert and Cameron Hummels for useful discussions. Support for PFH was provided by an Alfred P. Sloan Research Fellowship, NASA ATP Grant NNX14AH35G, and NSF Collaborative Research Grant #1411920 and CAREER grant #1455342. CCH is grateful to the Gordon and Betty Moore Foundation for financial support. CAFG was supported by NSF through grants AST-1412836 and AST-1517491, by NASA through grant NNX15AB22G, and by STScI through grants HST-AR- 14293.001-A and HST-GO-14268.022-A. DK was supported in part by NSF grant AST-1412153. Numerical calculations were run on the Caltech compute cluster "Zwicky" (NSF MRI award #PHY-0960291) and allocation TG-AST130039 granted by the Extreme Science and Engineering Discovery Environment (XSEDE) supported by the NSF.

REFERENCES

Agertz O., Kravtsov A. V., 2015, ArXiv e-prints, arXiv:1509.00853
Agertz O., Kravtsov A. V., Leitner S. N., Gnedin N. Y., 2013, ApJ, 770, 25
Beck A. M., Lesch H., Dolag K., Kotarba H., Geng A., Stasyszyn F. A., 2012, MNRAS, 422, 2152
Beck R., 2009, Astrophysics and Space Sciences Transactions, 5, 43
Beck R., Brandenburg A., Moss D., Shukurov A., Sokoloff D., 1996, ARA&A, 34, 155
Bernet M. L., Miniati F., Lilly S. J., Kronberg P. P., Dessauges-Zavadsky M., 2008, Nature, 454, 302
Booth C. M., Agertz O., Kravtsov A. V., Gnedin N. Y., 2013, ApJ, 777, L16
Bournaud F., Elmegreen B. G., Teyssier R., Block D. L., Puerari I., 2010, MNRAS, 409, 1088
Braginskii S. I., 1965, Reviews of Plasma Physics, 1, 205
Brüggen M., Scannapieco E., 2016, ArXiv e-prints
Ceverino D., Klypin A., 2009, ApJ, 695, 292
Choi E., Stone J. M., 2012, ApJ, 747, 86
Cole S., Lacey C. G., Baugh C. M., Frenk C. S., 2000, MNRAS, 319, 168
Cowie L. L., McKee C. F., 1977, ApJ, 211, 135
Dedner A., Kemm F., Kröner D., Munz C.-D., Schnitzer T., Wesenberg M., 2002, Journal of Computational Physics, 175, 645
Dobbs C. L., Burkert A., Pringle J. E., 2011, MNRAS, 413, 2935
Dong R., Stone J. M., 2009, ApJ, 704, 1309
Dubois Y., Teyssier R., 2010, A&A, 523, A72
Erb D. K., Steidel C. C., Shapley A. E., Pettini M., Reddy N. A., Adelberger K. L., 2006, ApJ, 646, 107
Evans, II N. J., 1999, ARA&A, 37, 311
Evans, II N. J. et al., 2009, ApJS, 181, 321
Faucher-Giguere C.-A., Feldmann R., Quataert E., Keres D., Hopkins P. F., Murray N., 2016, arXiv:1601.07188
Faucher-Giguère C.-A., Hopkins P. F., Kereš D., Muratov A. L., Quataert E., Murray N., 2015, MNRAS, 449, 987
Faucher-Giguère C.-A., Lidz A., Zaldarriaga M., Hernquist L., 2009, ApJ, 703, 1416
Faucher-Giguère C.-A., Quataert E., Hopkins P. F., 2013, MNRAS, 433, 1970
Federrath C., Klessen R. S., Schmidt W., 2008, ApJ, 688, L79
Federrath C., Sur S., Schleicher D. R. G., Banerjee R., Klessen R. S., 2011, ApJ, 731, 62
Genzel R. et al., 2008, ApJ, 687, 59
Governato F., Willman B., Mayer L., Brooks A., Stinson G., Valenzuela O., Wadsley J., Quinn T., 2007, MNRAS, 374, 1479
Harper-Clark E., Murray N., 2011, in IAU Symposium, Vol. 270, Computational Star Formation, Alves J., Elmegreen B. G., Girart J. M., Trimble V., eds., pp. 235–238
Hayward C. C., Hopkins P. F., 2015, ArXiv e-prints, arXiv:1510.05650
Hernquist L., 1990, ApJ, 356, 359
Hopkins P. F., 2013, MNRAS, 428, 2840
Hopkins P. F., 2015a, ArXiv e-prints, arXiv:1509.07877
Hopkins P. F., 2015b, MNRAS, 450, 53
Hopkins P. F., 2016, ArXiv e-prints
Hopkins P. F., Cox T. J., Hernquist L., Narayanan D., Hayward C. C., Murray N., 2013a, MNRAS, 430, 1901
Hopkins P. F., Kereš D., Murray N., Hernquist L., Narayanan D., Hayward C. C., 2013b, MNRAS, 433, 78
Hopkins P. F., Kereš D., Oñorbe J., Faucher-Giguère C.-A., Quataert E., Murray N., Bullock J. S., 2014, MNRAS, 445, 581
Hopkins P. F., Narayanan D., Murray N., 2013c, MNRAS, 432, 2647
Hopkins P. F., Narayanan D., Murray N., Quataert E., 2013d, MNRAS, 433, 69
Hopkins P. F., Quataert E., Murray N., 2011, MNRAS, 417, 950
Hopkins P. F., Quataert E., Murray N., 2012a, MNRAS, 421, 3522
Hopkins P. F., Quataert E., Murray N., 2012b, MNRAS, 421, 3488
Hopkins P. F., Raives M. J., 2016, MNRAS, 455, 51
Hu C.-Y., Naab T., Walch S., Glover S. C. O., Clark P. C., 2015, ArXiv e-prints, arXiv:1510.05644
Jansson R., Farrar G. R., 2012a, ApJ, 757, 14
Jansson R., Farrar G. R., 2012b, ApJ, 761, L11

Jun B.-I., Jones T. W., 1999, ApJ, 511, 774
Jun B.-I., Norman M. L., 1996a, ApJ, 472, 245
Jun B.-I., Norman M. L., 1996b, ApJ, 465, 800
Jun B.-I., Norman M. L., Stone J. M., 1995, ApJ, 453, 332
Kainulainen J., Tan J. C., 2013, A&A, 549, A53
Kannan R., Springel V., Pakmor R., Marinacci F., Vogelsberger M., 2016, MNRAS, 458, 410
Katz N., Weinberg D. H., Hernquist L., 1996, ApJS, 105, 19
Katz N., White S. D. M., 1993, ApJ, 412, 455
Kennicutt, Jr. R. C., 1998, ApJ, 498, 541
Kereš D., Katz N., Davé R., Fardal M., Weinberg D. H., 2009, MNRAS, 396, 2332
Kim C.-G., Ostriker E. C., 2015, ApJ, 815, 67
Kim C.-G., Ostriker E. C., Kim W.-T., 2013, ApJ, 776, 1
Kim C.-G., Ostriker E. C., Kim W.-T., 2014, ApJ, 786, 64
Kotarba H., Karl S. J., Naab T., Johansson P. H., Dolag K., Lesch H., Stasyszyn F. A., 2010, ApJ, 716, 1438
Kotarba H., Lesch H., Dolag K., Naab T., Johansson P. H., Donnert J., Stasyszyn F. A., 2011, MNRAS, 415, 3189
Kronberg P. P., Bernet M. L., Miniati F., Lilly S. J., Short M. B., Higdon D. M., 2008, ApJ, 676, 70
Kroupa P., 2002, Science, 295, 82
Krumholz M. R., Gnedin N. Y., 2011, ApJ, 729, 36
Krumholz M. R., Klein R. I., McKee C. F., 2011, ApJ, 740, 74
Kulsrud R. M., Zweibel E. G., 2008, Reports on Progress in Physics, 71, 046901
Leitherer C. et al., 1999, ApJS, 123, 3
Levine E. S., Blitz L., Heiles C., 2006, ApJ, 643, 881
Lilly D. K., 1967
Ma X., Hopkins P. F., Faucher-Giguere C.-A., Zolman N., Muratov A. L., Keres D., Quataert E., 2015, ArXiv e-prints, arXiv:1504.02097
Markevitch M., Vikhlinin A., 2007, PhysRep, 443, 1
Martizzi D., Fielding D., Faucher-Giguère C.-A., Quataert E., 2016, MNRAS
McCourt M., O'Leary R. M., Madigan A.-M., Quataert E., 2015, MNRAS, 449, 2
Merrifield M. R., 1992, AJ, 103, 1552
Molina F. Z., Glover S. C. O., Federrath C., Klessen R. S., 2012, ArXiv e-prints, arXiv:1203.2117
Muratov A. L., Kereš D., Faucher-Giguère C.-A., Hopkins P. F., Quataert E., Murray N., 2015, MNRAS, 454, 2691
Murray N., Ménard B., Thompson T. A., 2011, ApJ, 735, 66
Navarro J. F., Frenk C. S., White S. D. M., 1996, ApJ, 462, 563
Pakmor R., Springel V., 2013, MNRAS, 432, 176
Parrish I. J., McCourt M., Quataert E., Sharma P., 2012, MNRAS, 422, 704
Piontek R. A., Ostriker E. C., 2005, ApJ, 629, 849
Piontek R. A., Ostriker E. C., 2007, ApJ, 663, 183
Porter D. H., 1985, PhD thesis, California Univ., Berkeley
Powell K. G., Roe P. L., Linde T. J., Gombosi T. I., De Zeeuw D. L., 1999, Journal of Computational Physics, 154, 284
Reynolds C. S., McKernan B., Fabian A. C., Stone J. M., Vernaleo J. C., 2005, MNRAS, 357, 242
Robertson B. E., Kravtsov A. V., 2008, ApJ, 680, 1083
Ruszkowski M., Yang H.-Y. K., Zweibel E., 2016, arXiv:1602.04856
Salem M., Bryan G. L., Hummels C., 2014, ApJ, 797, L18
Sarazin C. L., 1988, X-ray emission from clusters of galaxies
Sharma P., Chandran B. D. G., Quataert E., Parrish I. J., 2009, ApJ, 699, 348
Sharma P., Parrish I. J., Quataert E., 2010, ApJ, 720, 652
Shen S., Wadsley J., Stinson G., 2010, MNRAS, 407, 1581
Shetty R., Ostriker E. C., 2008, ApJ, 684, 978
Sijacki D., Springel V., 2006, MNRAS, 371, 1025
Smagorinsky J., 1963, Monthly Weather Review, 91, 99
Somerville R. S., Primack J. R., 1999, MNRAS, 310, 1087
Sparre M., Hayward C. C., Feldmann R., Faucher-Giguère C.-A., Muratov A. L., Kereš D., Hopkins P. F., 2015, ArXiv e-prints, arXiv:1510.03869
Spitzer L., Härm R., 1953, Physical Review, 89, 977
Springel V., 2005, MNRAS, 364, 1105
Springel V., 2010, MNRAS, 401, 791
Springel V., Hernquist L., 2003, MNRAS, 339, 289
Stinson G. S., Brook C., Macciò A. V., Wadsley J., Quinn T. R., Couchman H. M. P., 2013, MNRAS, 428, 129
Stone J. M., Gardiner T. A., Teuben P., Hawley J. F., Simon J. B., 2008, ApJS, 178, 137
Tacconi L. J. et al., 2010, Nature, 463, 781
Tasker E. J., 2011, ApJ, 730, 11
Thacker R. J., Couchman H. M. P., 2000, ApJ, 545, 728
Thompson C., 2000, ApJ, 534, 915
Thompson T. A., Krumholz M. R., 2014, ArXiv e-prints, arXiv:1411.1769
Uhlig M., Pfrommer C., Sharma M., Nath B. B., Enßlin T. A., Springel V., 2012, MNRAS, 423, 2374
van de Voort F., Quataert E., Hopkins P. F., Kereš D., Faucher-Giguère C.-A., 2015, MNRAS, 447, 140
Wadsley J. W., Veeravalli G., Couchman H. M. P., 2008, MNRAS, 387, 427
Wang P., Abel T., 2009, ApJ, 696, 96
Widrow L. M., 2002, Reviews of Modern Physics, 74, 775
Wiersma R. P. C., Schaye J., Smith B. D., 2009a, MNRAS, 393, 99
Wiersma R. P. C., Schaye J., Theuns T., Dalla Vecchia C., Tornatore L., 2009b, MNRAS, 399, 574
Williams J. P., McKee C. F., 1997, ApJ, 476, 166
Zakamska N. L., Narayan R., 2003, ApJ, 582, 162
Zuckerman B., Evans, II N. J., 1974, ApJ, 192, L149
ZuHone J. A., Kunz M. W., Markevitch M., Stone J. M., Biffi V., 2015, ApJ, 798, 90

APPENDIX A: CONVERGENCE TESTS

We performed convergence tests using our isolated SMC model, varying the particle mass by 2 orders of magnitude (see Table A1). The HR run in Table A1 matches the resolution of the standard SMC runs in the main text.

The resulting SFRs are shown in Fig. A1, the phase structure and radial velocity distribution are shown in Fig. A2 and Fig. A3, respectively, and the turbulent and magnetic energies are shown in Fig. A4. The star formation rate inFig. A1 converges most rapidly with resolution. Among the inspected resolutions, there is little difference. As for the phase structure Fig. A2, the cold neutral and warm ionized gas have very similar density distributions at all the resolutions tested. The hot gas and outflow density distributions converge more slowly but appear to be converged when at the MR resolution (i.e. resolution elements of a few thousand solar masses), as does the radial velocity distribution of gas particles Fig. A3. Above this resolution, individual SN remnants begin to have their Sedov-Taylor phases resolved, and therefore generation of hot gas and outflows can be captured more robustly. The turbulent and magnetic energies similarly appear converged at the MR resolution. As the resolution increases, minor increases in the magnetic energy and minor decreases in the turbulent energy are found. This is because the small-scale shear field, which can dissipate turbulent kinetic energy and enhance the magnetic energy through field-line stretching, is suppressed at low resolution (Jun et al. 1995).

The convergence tests imply that our simulations of the more-massive galaxies, such as HiZ, Ell and CosmoMW, might not have sufficient resolution for all of their properties to be fully converged, especially their hot gas and outflow properties. Moreover, it is worth noting that, although we do not expect this to be the case, we cannot exclude the possibility of false convergence. The best resolution that we can achieve for galaxy simulations is inevitably many orders of magnitude coarser than the natural viscosity scale

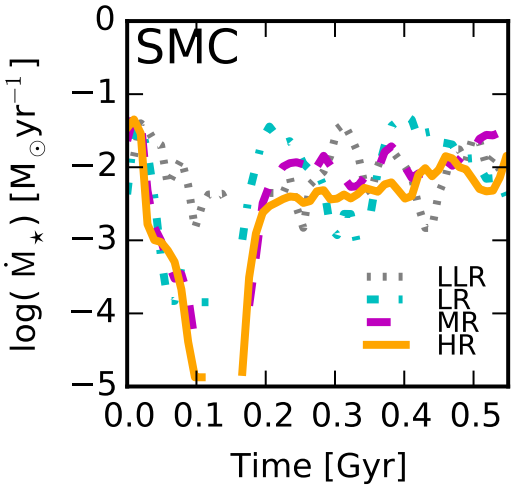

Figure A1. Convergence of the star formation rate of the SMC model. The star formation rate converges quickly. Even at a resolution 2 orders of magnitude lower than the standard resolution, the SFR has a similar quasi-equilibrium value, $\sim 0.01 M_\odot/yr$.

Table A1. Galaxy models used in our convergence tests

Initial Condition	Physics	Resolution	m_g	m_h	m_d	m_b
SMC	All Microphysics	LLR	3.6e4	2.9e5	6.2e4	4.8e4
SMC	All Microphysics	LR	3.6e3	2.9e4	6.2e3	4.8e3
SMC	All Microphysics	MR	1.1e3	8.6e3	1.9e3	1.4e3
SMC	All Microphysics	HR	3.6e2	2.9e3	6.2e2	4.8e2

(1) Initial Condition: Galaxy model used. These all adopt our SMC IC. (2) Physics: These all consider all microphysics, the most demanding case. (3) Resolution name. LLR: The lowest resolution. LR: Low resolution. MR: Medium resolution. HR: High resolution. (4) m_g: Gas particle mass. (5) m_h: Halo particle mass. (6) m_d: Stellar disk particle mass. (7) m_b: Bulge particle mass.

(the Kolmogorov length scale). Thus, it is possible that some important effects of fluid microphysics will appear only at much higher resolutions than these that will be achievable for galaxy simulations in the foreseeable future.

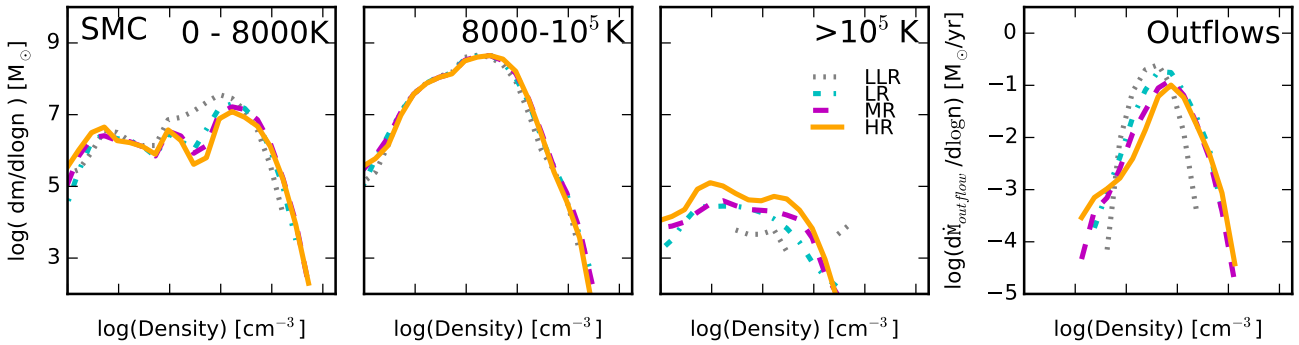

Figure A2. Convergence of the density distribution of gas in different phases in the SMC model. The cold neutral and warm ionized gas have very similar density distributions at all of the resolutions inspected. The properties of the hot gas and outflows, on the other hand, appear to require resolution elements of $\sim$ 1000 $M_\odot$ per gas particle, which roughly separates whether SNe are individually resolved. Nevertheless, the density distributions of the hot gas and outflows in the lower-resolution runs do not differ drastically from the converged values.

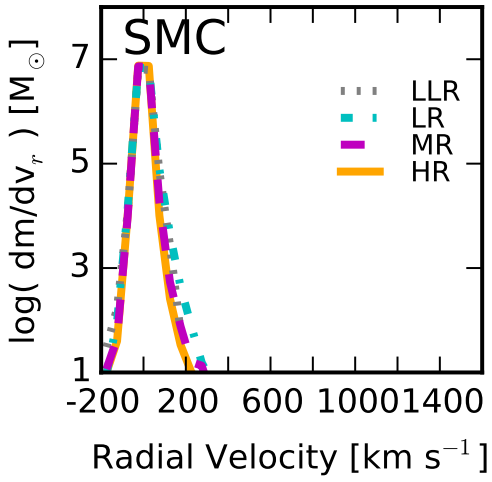

Figure A3. Convergence of the radial velocity distribution of the gas particles in the SMC model. For all of the tested resolutions, the gas particles have almost identical radial velocity distributions.

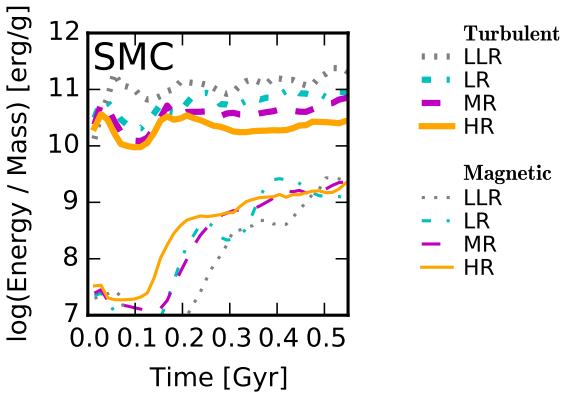

Figure A4. The total turbulent kinetic energy (*thick lines*; defined in § 4.4) and magnetic energy (*thin lines*) per unit mass of the non-outflowing disc gas in SMC. Both the magnetic and turbulent energies appear converged once the gas mass resolution is $\sim$ 1000 $M_\odot$.